KfK 4598
CNEA NT – 10/89
Juli 1989

Reaction Behaviour of B_4C Absorber Material with Stainless Steel and Zircaloy in Severe LWR Accidents

P. Hofmann, M. Markiewicz, J. Spino
Institut für Material- und Festkörperforschung
Projektgruppe LWR-Sicherheit

Kernforschungszentrum Karlsruhe

Kernforschungszentrum Karlsruhe
Institut für Material- und Festkörperforschung
Projektgruppe LWR-Sicherheit

KfK 4598
CNEA NT - 10/89

Reaction behaviour of B_4C absorber material with stainless steel and Zircaloy in severe LWR accidents

P. Hofmann, M. Markiewicz*, J. Spino*

*Comisión Nacional de Energia Atómica
Av. de Libertador 8250, 1429 Buenos Aires
Argentina

Kernforschungszentrum Karlsruhe GmbH, Karlsruhe

Als Manuskript vervielfältigt

Kernforschungszentrum Karlsruhe GmbH
Postfach 3640, 7500 Karlsruhe 1

ISSN 0303-4003

Reaction behaviour of B_4C absorber material with stainless steel and Zircaloy in severe LWR accidents

Abstract

The chemical reaction behaviour of B_4C absorber material with 1.4919 stainless steel (AISI 316) and Zircaloy-4 was studied in the temperature range 800 - 1600 °C. The reaction kinetics for both systems can be described by parabolic rate laws. Above 1000 °C, the reaction zone growth rates x^2/t in the B_4C/stainless steel system are by about two orders of magnitude higher than those in the B_4C/Zircaloy-4 system. The compatibility specimens are quickly and completely liquefied at about 1250 °C for the B_4C/stainless steel reaction couples and at about 1650 °C for the B_4C/Zircaloy-4 reaction couples. In both reaction systems the liquefaction occurs below the melting points of the components.

Reaktionsverhalten von B_4C Absorbermaterial gegenüber rostfreiem Stahl und Zircaloy bei schweren LWR-Störfällen

Zusammenfassung

Es wurde das chemische Reaktionsverhalten von B_4C Absorbermaterial gegenüber 1.4919 rostfreiem Stahl (AISI 316) bzw. Zircaloy-4 im Temperaturbereich von 800 bis 1600 °C untersucht. Die Reaktionskinetik kann für beide Systeme durch parabolische Zeitgesetze beschrieben werden. Oberhalb 1000 °C sind die Wachstumsraten x^2/t der Reaktionszonen für das System B_4C/rostfreier Stahl etwa zwei Größenordnungen größer als die für das Reaktionssystem B_4C/Zircaloy-4. Die B_4C/rostfreier Stahl-Verträglichkeitsproben schmelzen oberhalb etwa 1250 °C und die des Systems B_4C/Zircaloy-4 oberhalb 1650 °C schnell und vollständig zusammen. In beiden Reaktionssystemen erfolgt die Verflüssigung der Proben unterhalb dem Schmelzpunkt der Komponenten.

Contents

1. Introduction

The absorber rods in Boiling Water Reactors (BWR) and in Fast Breeder Reactors (FBR) consist of boron carbide (B_4C) pellets or B_4C powder in stainless steel tubes. In the case of BWRs, the absorber rods are contained in a four-bladed stainless steel assembly. Four fuel rod bundles are each surrounded by a Zircaloy channel box arranged around the cross-shaped control element (fig. 1). The system boron carbide/stainless steel tube is not stable thermodynamically, i.e. chemical interactions have to be expected. Under normal reactor operation conditions the limited chemical interactions between B_4C and stainless steel can be tolerated. But the question is how the absorber rods behave chemically at temperatures beyond 1000 °C which have to be assumed in severe reactor accidents. First scoping tests with small LWR fuel rod bundles containing B_4C absorber rods showed strong chemical interactions at temperatures above 1250 °C which resulted in a fast liquefaction and subsequent relocation of the absorber rod material [1]. The liquid B_4C/stainless steel reaction products then interact with the Zircaloy flow channel box and the adjacent UO_2/Zircaloy fuel rods (fig. 1). For this reason, it is also of interest to study the chemical interactions between B_4C and Zircaloy.

The objective of this paper is to describe quantitatively the chemical interaction between B_4C and stainless steel as well as between B_4C and Zircaloy up to the liquefaction of the reaction specimens. The possible chemical interactions between the stainless steel absorber blade and the Zircaloy channel box and fuel rod cladding are not part of this work. Such results will be described elsewhere [2]. The results of these single effects tests are important to understand and to describe the complex material behaviour in integral experimentes like the CORA fuel rod bundle meltdown tests [3].

In the literature, a few results of B_4C/stainless steel reaction experiments, performed with FBR absorber rods, have been published [4,5,6]. In some of these experiments sodium was used as bonding material between the B_4C and stainless steel which improves the heat transfer from the B_4C to the coolant. However, at the same time, sodium bonding enhances the absorber material/cladding chemical interactions [6].

2. Materials and conduct of the experiments

The isothermal annealing tests were performed with 1.4919 (AISI 316) stainless steel (ss) and Zircaloy-4 (Zry) capsules which were filled with B_4C powder. To get a good solid-state contact between B_4C and the capsule walls, the powder was pressed into the crucible-like capsules. After that, the capsules were closed gas-tight by a conical plug. The preparation and the closure of the specimens were performed in a glove box under inert gas conditions.

Some preliminary compatibility tests were performed at 1100 °C with B_4C powders of various particle sizes to determine if the particle size influences the extent of the chemical interactions. No influence of particle size over the range from 44 to 840 µm on the interaction could be determined using the four different powder mixtures. A particle size ranging from 177 to 250 µm was finally selected for the compatibility experiments; the chemical composition of the powder was: C = 20.9, N = 0.39, and O = 0.19 wt.%, the remainder was boron.

The annealing experiments were performed in a tube furnace under flowing argon. For the B_4C/ss reaction couples the investigated temperature range varied between 800 and 1200 °C and for the B_4C/Zry reaction couples between 800 and 1600 °C. The annealing times ranged from 5 minutes to 300 hours. The maximum temperatures of 1200 and 1600 °C, respectively, for the reaction couples were limited by the onset of liquid phase formation at these temperatures and the subsequent fast and complete liquefaction of the specimens at slightly higher temperatures.

After the annealings, the specimens were mechanically cut and then metallographically prepared for examinations of the reaction zones with an optical microscope. The thickness of the reaction zones were measured at four different locations of the B_4C/metal interface. In addition, some Scanning Electron Microscopy (SEM)/Energy Dispersive X-Ray (EDX) or SEM/Wave Length Dispersive X-Ray (WDX) and Auger Electron Spectroscopy (AES) examinations were made to obtain information on the chemical compositions of the reaction products and diffusion zones. In a few cases, microhardness measurements were made to determine the extent of the diffusion zone.

3. Results

3.1 Chemical interactions between B_4C and stainless steel

3.1.1 Morphology of the interaction zone and reaction kinetics

The chemical interaction between B_4C and stainless steel resulted in the formation of two reaction layers. The first, adjacent to the B_4C absorber material, was very thin and had a rather homogeneous appearance; the second reaction layer was much thicker and was characterized by the presence of a great amount of second-phase precipitation in the ss matrix, mainly along the grain boundaries. Fig. 2 shows the appearance of both reaction layers at 1000 °C after 300 hours. A similar sequence of reaction layers was observed at 1100 °C. At 1200 °C, however, the appearance of the reaction layer changed noticeably (fig. 3). In the first reaction layer many macrovoids and in the second reaction layer numerous microvoids have developed. In the chemically attacked steel matrix the onset of eutectic melting was observed at some locations (fig. 4).

In order to determine the B_4C/ss reaction kinetics, the total reaction zone thickness of both reaction layers was determined as a function of temperature and time. The results are listed in table 1. The isothermal growth of the reaction layer thickness is a linear function of the square root of time (parabolic rate law) for all temperatures examined (fig. 5). This is an indication of a diffusion-controlled chemical interaction. The reaction zone growth rates for the B_4C/ss chemical interactions are listed in table 2. These data are plotted as a function of the reciprocal temperature together with some literature data in fig. 6 [5,6]. The growth rate equation determined for the temperature range 800 - 1200 °C is:

$$x^2/t\ (cm^2/s) = 8.76 \cdot 10^6 \exp(-378000/RT) \qquad (1)$$

$$R = 8.314\ J/mol \cdot K$$

This equation cannot be extrapolated to higher temperatures. Above 1200 °C, the liquid phase formation starts. At about 1250 °C the B_4C/ss reaction specimens became completely liquefied within a few seconds as a result of eutectic interactions.

3.1.2 Chemical characterization of the reaction layers

The reaction zones of the specimens were examined by Auger Electron Spectroscopy. Besides the determination of the element distribution, quantitative measurements were performed. Some typical results of a specimen annealed at 1200 °C for 6 hours are shown in fig. 7. As can be recognized easily, the first reaction layer consists mainly of a (Fe,Cr) boride phase; the Fe and C dot maps are not shown. The chemical composition of this boride phase is $FeCr_{0.89}B_{1.15}$. The (Fe,Cr) boride precipitates in the second reaction layer have a different chemical composition which varies between $FeCr_{1.1}B_{0.97}$ and $FeCr_{1.6}B_{1.4}$. The boride precipitates within the second reaction layer contained small amounts of carbon whereas the first reaction layer was free of any carbon.

The stainless steel matrix adjacent to the first reaction layer was depleted in Cr and enriched in Ni (fig. 7). Similar observations were made in previous experiments [4,6]. The amount of (Fe,Cr) boride precipitates within the second reaction layer decreases with increasing distance from the B_4C/ss interface. At the same time, the Ni content within the attacked ss matrix decreases and finally reaches its initial value. The reason for this behaviour may be the low solubility of Ni in the boride phase [4] and the reduced affinity of Ni to boron compared to that of Cr and Fe. The strong Cr depletion of the ss matrix is caused by the (Fe,Cr) boride formation.

No carbon could be detected in the first reaction layer and neither in the ss matrix of the second reaction layer. Only small amounts of C could be analyzed in the (Fe,Cr) boride precipitations of the second reaction layer. Similar observations are described in [6].

To determine the influence and depth of boron diffusion into the ss matrix microhardness measurements were performed. The result of one specimen is depicted in fig. 8. The first reaction layer shows a pronounced increase in microhardness of about 1750 kp/mm^2 compared to that of the unreacted ss matrix of about 200 kp/mm^2. The average microhardness of the second reaction layer is about 420 kp/mm^2. The overall thickness of the reaction zones determined by microhardness measurements is about 900 µm (fig. 8) compared to 950 µm determined metallographically (table 1). In the literature [7], a microhardness of 2160 kp/mm^2 was measured for (Fe,Cr)B and 1750 kp/mm^2 for the compound $(Fe,Cr)_2B$. The microhardness results provide support along with

our quantitative chemical results for a metal to boron ratio of about 2 for the borides in the first reaction layer. The formation of a $(Fe,Cr)_2B$ compound as a result of chemical interactions between B_4C and stainless steel was also demonstrated by other authors [4] by X-ray diffraction measurements.

3.2 Chemical interactions between B_4C and Zircaloy-4

3.2.1 Morphology of the interaction zone and reaction kinetics

The chemical interactions between B_4C and Zircaloy-4 resulted in the formation of different types of reaction zones in the temperature regions 800 - 1100 °C, 1200 - 1500 °C, and 1600 °C and at slightly higher temperatures. At about 1650 °C, the compatibility specimens were completely liquefied during heatup. Between 800 and 1100 °C one reaction layer formed which consisted of a mixture of zirconium boride and zirconium carbide (fig. 9). In the temperature range of 1200 to 1500 °C two reaction layers formed (fig. 10). The reaction layer adjacent to the B_4C/Zry interface was similar in composition to that at lower temperatures, i.e. it consisted of zirconium boride and zirconium carbide. The subsequent reaction layer, in the direction of the unreacted Zry matrix, consisted mainly of zirconium boride (fig. 10). At 1600 °C, also two reaction layers formed, but, in addition, the onset of a localized liquid phase and zirconium-carbide precipitation in the Zry matrix could be observed (fig. 11). The precipitates were distributed over the whole Zry annealing capsule cross-section up to the outer diameter. For this reason, the thickness of the second reaction layer could not be determined at 1600 °C, not even after 5 minutes annealing time, since it extended up to the outer surface of the wall. The precipitates within the Zry matrix were surrounded by a thin second phase which formed probably during cooling (fig. 12). As already mentioned, at temperatures ≥ 1650 °C a sudden meltdown of the B_4C/Zry specimens occurred.

To determine the reaction kinetics between B_4C and Zircaloy-4 the thickness of the total reaction zone was measured as a function of the reaction time up to temperatures of 1500 °C. At 1600 °C only the thickness of the first reaction layer could be determined. The results are listed in table 3 and plotted in figs 13, 14, and 15 versus the square root of the reaction time. Also in the B_4C/Zry reaction couple, the growth of the reaction layers obeys parabolic rate laws indicating that the rate-controlling step of the interactions is a diffusion process. The

calculated isothermal growth rates are listed in table 4 and plotted versus the reciprocal temperature in fig. 16. As can be recognized, the slope of the Arrhenius plot, e.g. the activation energy, changes at temperatures above 1500 °C to much higher values. The reason may be the formation of small amounts of liquid phases. However, the metallographic detection of this phase was not unambigous. The determined growth rate equations for 800 - 1500 °C are (table 5):

$$x^2/t\,(cm^2/s) = 4.15 \cdot 10^6 \exp(-122650/RT) \qquad (2)$$

and for 1500 - 1600 °C

$$x^2/t\,(cm^2/s) = 7.94 \cdot 10^{33} \exp(-1438300/RT) \qquad (3)$$

$$R = 8.314\ J/mol \cdot K$$

The slope of the Arrhenius plot between 1500 and 1600 °C should actually be even steeper, since the thickness of the second reaction layer was not considered at 1600 °C because it could not be determined

3.2.2 Chemical characterization of the reaction layers

Only semi-quantitative AES and SEM examinations of the reaction zones have been performed. The results of a specimen annealed at 1500 °C for 1 h are shown in fig. 10. The first reaction layer consists of a mixture of ZrC and ZrB_2 and the second reaction layer mainly of ZrB_2. The same results have been obtained at 1600 °C but at this temperature zirconium carbide precipitates formed in addition in the Zry matrix (fig. 12). The ZrC precipitates were partially surrounded by another phase of different chemical composition which probably formed during cooldown of the specimens due to changes in the carbon solubility of the precipitates with temperature. The ternary Zr-B-C phase diagrams at 1400 and 1800 °C show that the equilibrium phases which form as a result of the B_4C/Zry interaction should be ZrC and ZrB_2 (fig. 17).

4. Discussion

4.1 B_4C/stainless steel reaction system

The chemical interactions between B_4C and stainless steel and B_4C and Zircaloy-4 can be described by parabolic rate laws in the temperature ranges 800 - 1200 and 800 - 1600 °C, respectively, i.e. diffusion processes are the rate determining steps. In the case of the B_4C/ss reaction system, the chemical interactions above 800 °C are much faster than in the B_4C/Zry reaction system (fig. 19) and the reaction-zone growth rates differ from each other by up to about two orders of magnitude. Whereas for the B_4C/ss system the reaction can be described by one single Arrhenius equation, in the B_4C/Zry system two equations are necessary (table 5). The change to higher values in the apparent activation energy of the Arrhenius equation is probably caused by the formation of liquid phases which accelerate the extent of interaction. The pronounced temperature sensitivity of the reaction above 1500 °C is apparently determined by the increase in the amount of liquid phases which, finally, results in a complete liquefaction of the B_4C/Zry specimens above 1650 °C.

A comparison of our reaction zone growth data for the system B_4C/ss with literature data [5,6] is shown in fig. 6. As can be seen, our reaction kinetics data result in reaction zone growth rates x^2/t which are somewhat more than two orders of magnitude smaller. The reasons for this large difference may be the very high contact pressure (21 MPa) that was applied in [5] to increase and to maintain the solid-solid contact between B_4C and stainless steel during the annealing process, or the influence of liquid Na which was used as a bonding medium in [6]. Na plays an important role with respect to the transport of carbon and/or boron from the B_4C to the stainless steel. The B_4C/ss contact area will be enlarged by Na bonding. The literature reaction zone growth rate data [5,6] therefore define the upper limit for the extent of the chemical B_4C/ss interactions. The different chemical compositions of the examined stainless steels probably play only a minor role. But this could mean that in our case the rate determining step of the B_4C/ss interactions is the transport of C and B to the stainless steel surface, i.e. the quantity, and not the diffusion of the light elements through the reaction layer into the stainless steel matrix. However, with respect to the solid state contact conditions in LWR absorber elements the results obtained in our experiments are more representative.

The chemical analytical examinations of the reaction zones of the system B_4C/ss did not show any C diffusion into the first reaction layer adjacent to the B_4C. Some low C concentration could be noticed in the (Fe,Cr) boride precipitates within the second reaction layer but not in the surrounding stainless steel matrix. These results suggest therefore that the formation of the compact (Fe,Cr) boride phase at the B_4C/ss interface inhibited the diffusion of carbon into the stainless steel matrix and that the small quantities of C analyzed in the precipitates have their origin in the initial carbon content of the steel matrix and not from the B_4C. These observations are in agreement with those of reference [6] for the B_4C/ss 1.4970 and B_4C/ss 1.4981 reaction systems with sodium bonding.

In general, boron diffusion is much faster than that of carbon (fig. 19) [9,10]. In addition, the formation of stainless-steel-component borides is more stable thermodynamically than the corresponding carbides [6,11,12]. In fig. 19 the reaction zone growth rates of the B_4C/ss 1.4919 system are plotted as a function of the reciprocal temperature and compared with literature data on the diffusion coefficient of boron in Armco iron [10] and of carbon in stainless steel AISI 316 [9]. There are no data available on the diffusion of B in stainless steel. Apparently, the diffusion of B or C into stainless steel is not the rate determining step of the B_4C/ss interaction but the diffusion of B through the homogeneous-looking (Fe,Cr) boride phase, which forms the first reaction layer at the B_4C/ss interface. The average chemical composition of this phase is $FeCr_{0.89}B_{1.15}$, i.e. it is of the Fe_2B or Cr_2B type, which is in agreement with the ternary Fe-C-B and Cr-C-B phase diagrams (fig. 20).

The (Fe,Cr) boride reaction layer also plays an important role with respect to the critical upper temperature of the B_4C/ss material combination at which the formation of liquid phases occurs as a result of eutectic interactions. At about 1250 °C, a sudden and complete liquefaction of the B_4C/ss specimens takes place, which is of great importance with respect to safety considerations of LWRs. Above 1250 °C, the cruciform absorber element will be partially liquefied, the molten phases will relocate and form blockages at lower cooler elevations. Since ternary Fe(Cr)-C-B phase diagrams are only available up to 1100 °C (fig. 20) [15], the binary phase diagrams Fe-B, Cr-B, and Ni-B have to be used to explain the low-temperature liquefaction process (fig. 21). The eutectic temperature of the Fe-Fe_2B subsystem is 1174 °C and that of the Cr-Cr_2B subsystem is 1630 °C. In the Ni-B system first liquid phases form already at about 1020 °C. Taking into account the conditions in the B_4C/ss reaction system which resulted in the formation of a

$(Fe,Cr)_2B$ phase in contact with a modified steel matrix of high Ni and low Cr content, together with the binary phase diagram information, an eutectic temperature around 1250 °C, as experimentally observed, seems to be plausible. This failure temperature is about 200 °C lower than the melting point of stainless steel and about 850 °C lower than that of B_4C.

4.2 B_4C/Zircaloy-4 reaction system

Contrary to the B_4C/ss system, for which only the diffusion of B into the reaction layer and the steel matrix is of importance, B and C both diffuse into the Zry and interact chemically with Zr in the B_4C/Zry system (fig. 10). However, C diffuses deeper into the Zry matrix and in larger quantities than B forming ZrC precipitates. Zr has a higher solubility for C than for B (fig. 22) [13].

The slope of the Arrhenius equation for the temperature range 800 - 1500 °C deviates below 1100 °C somewhat from the experimental data points (fig. 16). The reason may be that below 1100 °C only one reaction layer ($ZrC + ZrB_2$) is formed whereas between 1100 and 1500 °C an additional reaction layer (ZrB_2) develops (fig. 10). The drastic change of the apparent activation energy at 1500 °C to a much higher value may be explained by the localized formation of liquid phases. There are ternary Zr-B-C phase diagrams only available for 1400 and 1800 °C (fig. 17) [8], they show liquid phases at 1800 °C but not at 1400 °C. The binary phase diagrams Zr-B and Zr-C have eutectic temperatures of about 1680 and about 1823 °C, respectively (fig. 22), i.e. well above 1500 °C. The complete and rapid liquefaction of the B_4C/Zry reaction specimens at about 1650 °C may be explained by the Zr-ZrB_2 eutectic temperature of 1680 °C and the pseudo binary Zr-$(B_{0.5}C_{0.5})$ phase diagram (fig. 23) [8], which shows that in the ternary Zr-B-C system liquid phases form already at about 1615 °C under equilibrium conditions. Since in our experiments Zircaloy-4 and not pure Zr was used, which contains about 1.5 wt.% Sn, some changes in the onset of liquid phase formation have to be expected in addition.

The ternary Zr-B-C equilibrium phase diagram (fig. 17) can be used in a first approach to obtain information on the reaction layer sequence. The tie line 1 → 2 represents the initial Zr/B_4C material contact of the reaction system. According to this tie line the reaction layer sequence from the B_4C to the Zry should be

$$B_4C \rightarrow [ZrB_2 + C] \rightarrow [ZrC + ZrB_2] \rightarrow Zry.$$

The experiments, however, show exactly the opposite reaction layer sequence (fig. 10). In our short-time experiments we were far away from equilibrium conditions and obtained, therefore, only intermediate conditions, which are not reflected in phase diagrams. Another reason could be the different diffusion velocities of B and C in the Zry matrix and the resulting reaction products.

4.3 LWR related safety aspects

The experimental results show that the complete failure of the B_4C/Zry reaction couple as a result of liquefaction occurs at about 1650 °C, which is 400 °C higher than that of the B_4C/ss reaction system at about 1250 °C. If Zircaloy would be used for the cruciform absorber element instead of stainless steel, the onset of liquid phase formation could be shifted to much higher temperatures. Besides, at temperatures below 1200 °C the B_4C/Zry reaction rate is much slower than that of B_4C/ss. Therefore, more time would be available during a severe accident for accident management measures.

Also, the use of different structural materials in large quantities within the reactor core, like Zircaloy and stainless steel, as it is the case in Boiling Water Reactors (BWR), causes additional severe material problems. Zircaloy and stainless steel interact eutectically with each other and liquid phases can form already below 1000 °C. However, below 1000 °C the reaction rate is rather slow, but it becomes much faster above 1000 °C [2]. At temperatures beyond 1250 °C a sudden liquefaction of the components takes place, if they are in contact with each other. ZrO_2 oxide layers on the Zircaloy surface of up to 50 µm thickness delay slightly the liquefaction but they are not able to prevent it [2]. Due to these interactions (B_4C/ss and Zry/ss) B_4C may come into contact with liquid and/or solid Zircaloy above 1250 °C.

The premature low-temperature failure of the BWR absorber element and its relocation may result in an early localized relocation of the B_4C absorber material within the reactor core and may cause local criticality problems in a severe reactor accident. In the CORA 16 experiment, in which a BWR fuel rod bundle was heated out-of-pile up to 2000 °C the failure of the absorber element and its relocation between 1200 and 1300 °C could be confirmed a long time before the fuel rods failed [3].

5. Summary and conclusions

- B_4C absorber material in contact with stainless steel or Zircaloy-4 will result in chemical interactions which can be described by parabolic rate laws.

- Above 1000 °C, the reaction zone growth rates x^2/t for the B_4C/stainless steel interactions are about two orders of magnitude larger than those for the B_4C/Zircaloy-4 interactions.

- In the B_4C/stainless steel reaction couple the reaction kinetics becomes very rapid near 1200 °C due to the formation of liquid phases. Beyond 1250 °C a sudden and complete liquefaction of the compatibility specimens takes place.

- Complete liquefaction of the B_4C/Zircaloy compatibility specimens occurs at about 1650 °C, i.e. at a temperature level 400 °C higher than that of the B_4C/stainless steel specimens.

- In both reaction systems the liquefaction occurs below the melting points of the components due to eutectic interactions.

- The premature low-temperature failure of the BWR absorber element and the localized relocation of B_4C within the reactor core may cause recriticality problems.

- With respect to the LWR core material behaviour in severe reactor accidents the use of Zircaloy cladded B_4C absorber material instead of stainless steel would result in a greater flexibility concerning accident management measures, because the meltdown occurs at higher temperatures which will be reached later.

Acknowledgement

We would like to thank Prof. Dr. W. Dienst (KfK) and Dr. R:R. Hobbins (EG + G Idaho) for their thorough technical and editorial revies of the manuscript.

We would also like to thank Mr. H. Metzger for the preparation of the metallographic specimens, Mr. J. Burbach for the SEM, and Mr. E. Nold for the

AES examinations. The work was sponsored by the "LWR Safety Project Group" (PRS/KfK).

6. References

[1] S. Hagen, P. Hofmann;
Physical and chemical behavior of LWR fuel elements up to very high temperatures.
KfK report 4104 (1987).

[2] P. Hofmann, M. Markiewicz;
Chemical interactions between Zircaloy and stainless steel or Inconel above 1000 °C.
To be published.

[3] S. Hagen, P. Hofmann, G. Schanz, L. Sepold;
Behavior of B_4C absorber material in Zircaloy/UO_2 fuel rod simulator bundles at high temperatures (CORA 16).
To be published, KfK report 4560.

[4] S. Ihara, K. Tanaka, M. Kojima, Y. Akimoto;
Study on the compatibility between B_4C and stainless steel.
IAEA-IWGFR Specialists Meeting on "Development and Application of Absorber materials", Dimitrovgrad, USSR, June 3 - 8, 1973, pp. 201 - 228.

[5] R.E. Dahl;
Boron carbide development of FFTF control elements.
ibid, pp. 107 - 128.

[6] H.J. Heuvel, P. Höller, P. Dünner;
Absorber material cladding chemical interaction in vented FBR absorber pins.
J. Nucl. Mater. 130 (1985) pp. 517 - 523.

[7] C. Badini, C. Gianoglio, G. Pradelli;
Preferential distribution of Cr and Ni in the borided layer obtained on synthetic Fe-Cr-Ni alloys.
J. Mater. Science 21 (1986) pp. 1721 - 1729.

[8] E. Rudy;
Ternary phase equilibria in transition metal-B-C-Si systems. Part V: Compendium of phase diagram data.
Technial Report AFML-TR-65-2, Part V (1969).

[9] R.P. Agarwala, M.C. Naik, M.S. Anand, A.R. Paul;
Diffusion of C in stainless steels.
J. Nucl. Mater. 36 (1970) pp. 41 - 47.

[10] H. Kunst, O. Schaaber;
Beobachtungen beim Oberflächenborieren von Stahl.
Härterei-Technische Mitteilungen 22 (1967) pp. 1 -25.

[11] I. Barin, O. Knacke;
Thermodynamic Properties of Inorganic Substances.
Springer Verlag (1973).

[12] I. Barin, O. Knacke, O. Kubaschewski;
ibid, Supplement, Springer Verlag (1977).

[13] T.B. Massalski;
Binary alloy phase diagrams, Vol. 1, 2
American Society for Metals, Ohio (1986).

[14] H. Kaneko, T. Nishizawa, T. Chiba;
Borides in stainless steel.
J. Japan Inst. of Metals 30/2 (1966) pp. 157 - 163.

[15] D. Lange;
Verschleißfeste Werkstoffe auf Borkarbidbasis.
KfK report 4009 (1985).

List of Tables

Table 1: Measured total reaction zone thickness for the diffusion couple B_4C/stainless steel 1.4919 (AISI 316) as a function of temperature and time.

Specimen	Temperature °C	Time h	Reaction zone thickness µm
66	800	25	4
67	"	100	10
68	"	300	21
70	900	25	20
71	"	100	37
72	"	300	137
73	1000	25	142
74	"	25	182
75	"	100	292
85	"	100	287
76	"	300	520
78	1100	6	250
61	"	25	590
77	"	100	1150
82	1200	1,5	387
83	"	6	950
84	"	25	1787

Table 2: Reaction zone growth rate for the diffusion couple B_4C/stainless steel 1.4919 (AISI 316) as function of temperature (800 - 1200 °C).

Temperature °C	Reaction zone growth rate, x^2/t cm^2/sec
800	3.65×10^{-12}
900	1.25×10^{-10}
1000	2.48×10^{-9}
1100	3.67×10^{-8}
1200	3.62×10^{-7}

Table 3: Measured total reaction zone thickness for the diffusion couple B_4C/Zircaloy-4 as a function of temperature and time.

Specimen	Temperature °C	Time h	Reaction zone thickness µm
86	800	6	4
87	800	25	10
88	800	100	18
89	800	500	52
90	900	6	5
93	900	25	8
92	900	100	15
91	900	300	26
94	1000	6	10
95	1000	25	14
96	1000	100	26
97	1000	300	42
100	1100	6	16
98	1100	25	20
101	1100	300	107
102	1200	6	29
104	1200	25	51
103	1200	100	77
106	1300	1.5	25
107	1300	6	39
108	1300	25	61

Table 3: continued

Specimen	Temperature °C	Time h	Reaction zone thickness µm
112	1400	1.5	26
111	1400	6	42
113	1400	25	75
147	1500	0.083	13
148	1500	0.25	19
149	1500	0.50	23
118	1500	1	34
150	1600	0.083	145
151	1600	0.25	255
152	1600	0.50	342
153	1600	1	450

Table 4: Reaction zone growth rate for the diffusion couple B_4C/Zircaloy-4 as function of temperature (800 - 1600 °C).

Temperature °C	Reaction zone growth rate, x^2/t cm^2/sec
800	1.11×10^{-11}
900	6.61×10^{-12}
1000	1.80×10^{-11}
1100	1.01×10^{-10}
1200	1.96×10^{-10}
1300	4.89×10^{-10}
1400	6.83×10^{-10}
1500	3.35×10^{-9}
1600	6.13×10^{-7}

Table 5: Growth rate equations for the diffusion couples B_4C/stainless steel 1.4919 (AISI 316) and B_4C/Zircaloy-4.

Reaction couple	Temperature range °C	Growth rate equation, x^2/t cm^2/sec
B_4C/ss 1.4919	800 - 1200 °C	$8.76 \times 10^6 \exp(-378000/RT)$
B_4C/Zircaloy-4	800 - 1400 °C	$4.15 \times 10^{-6} \exp(-122650/RT)$
B_4C/Zircaloy-4	1500 - 1600 °C	$7.94 \times 10^{33} \exp(-1438300/RT)$

List of Figures

Fig. 21: Binary alloy phase diagrams of the systems Fe-B, Cr-B, and Ni-B [13].

Fig. 22: Binary alloy phase diagrams of the systems Zr-B and Zr-C [13].

Fig. 23: Phase relations in the pseudo binary phase system Zr-($B_{0.5}C_{0.5}$) [8].

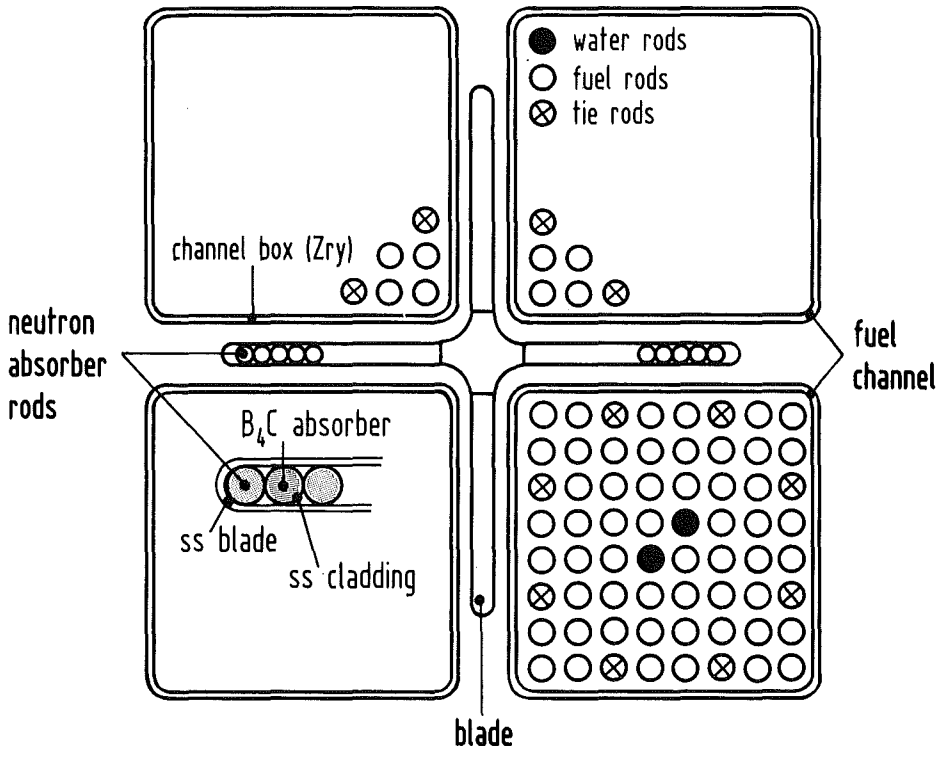

BWR cruciform control element

Fig. 1: Arrangement of the cruciform absorber blade in BWR fuel elements

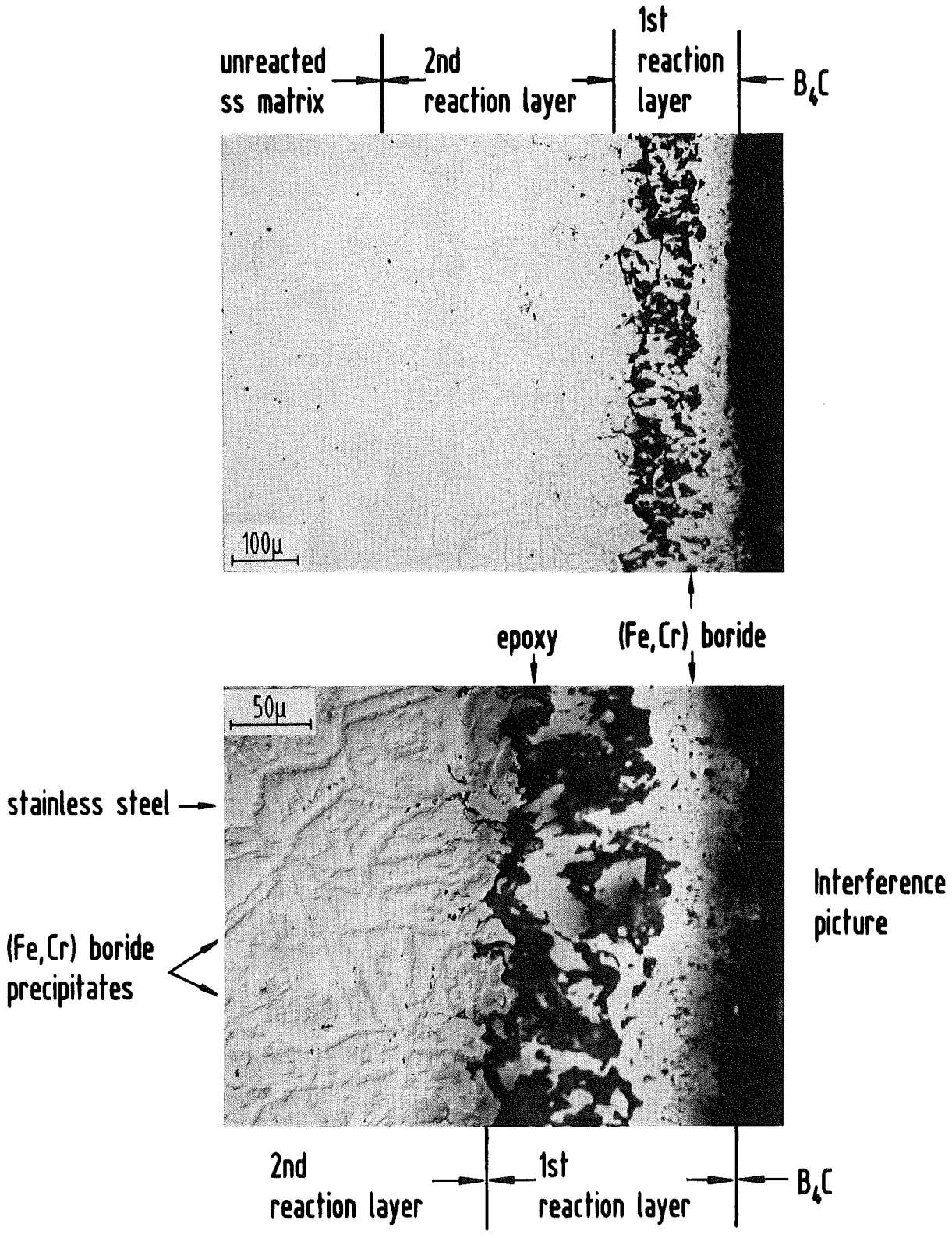

Fig. 2: B_4C/stainless steel 1.4919 (AISI 316) reaction layers after 300 h at 1000 °C.

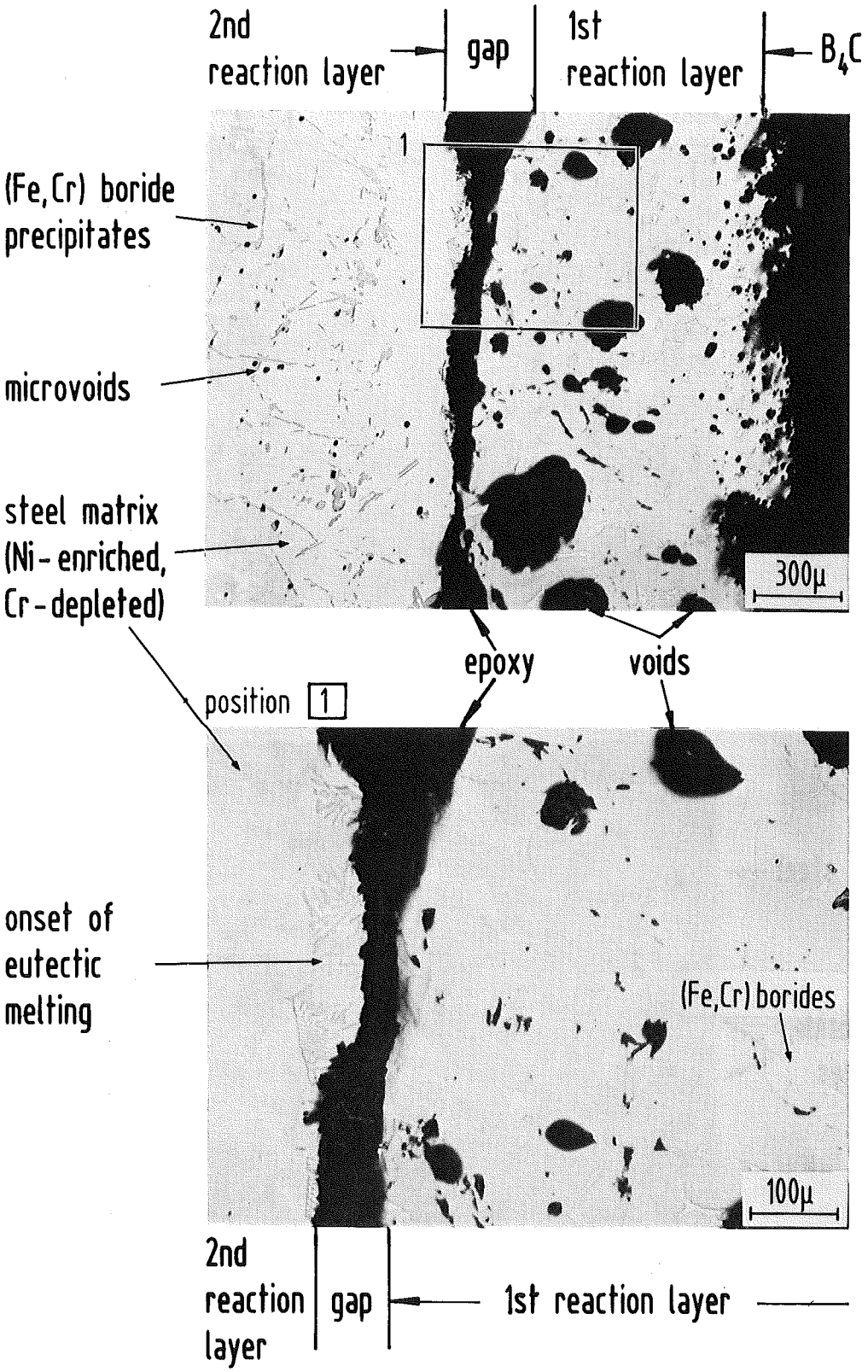

Fig. 3: B_4C/stainless steel reaction layers after 25 h at 1200 °C.

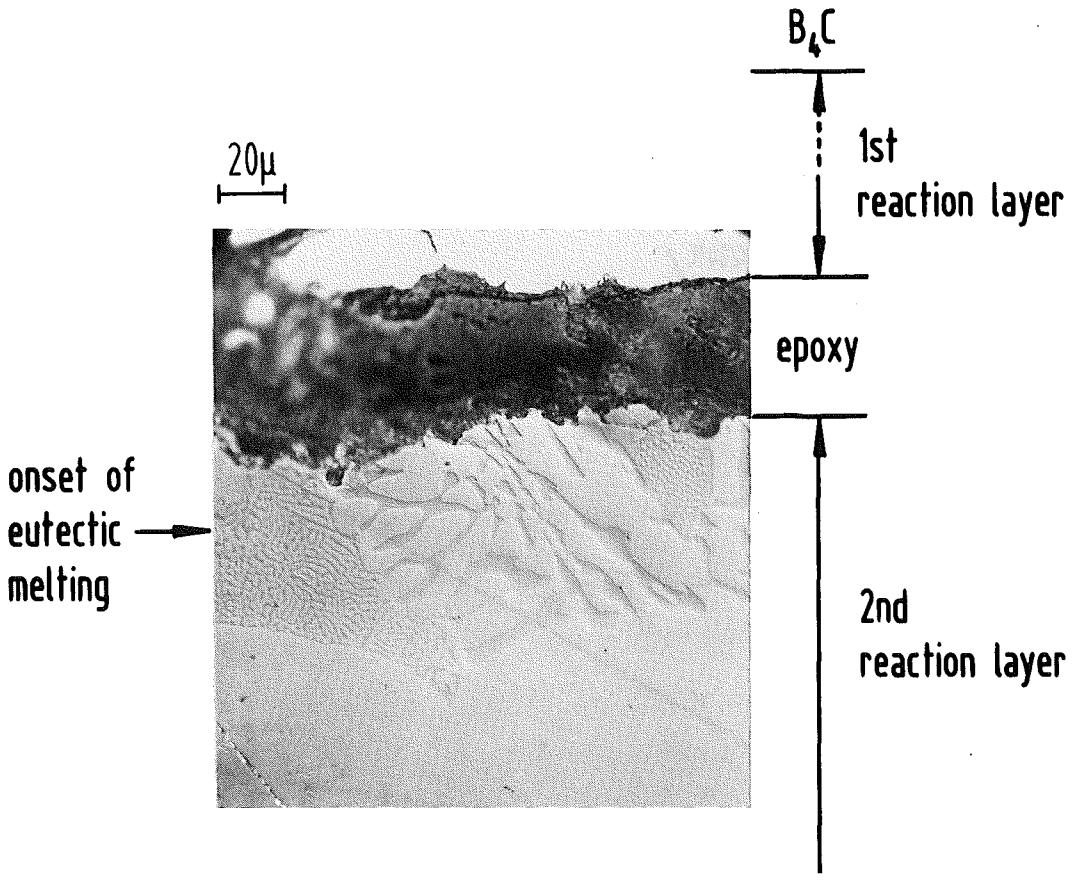

Fig. 4: B_4C/stainless steel reaction layers after 25 h at 1200 °C. Localized formation of liquid phases.

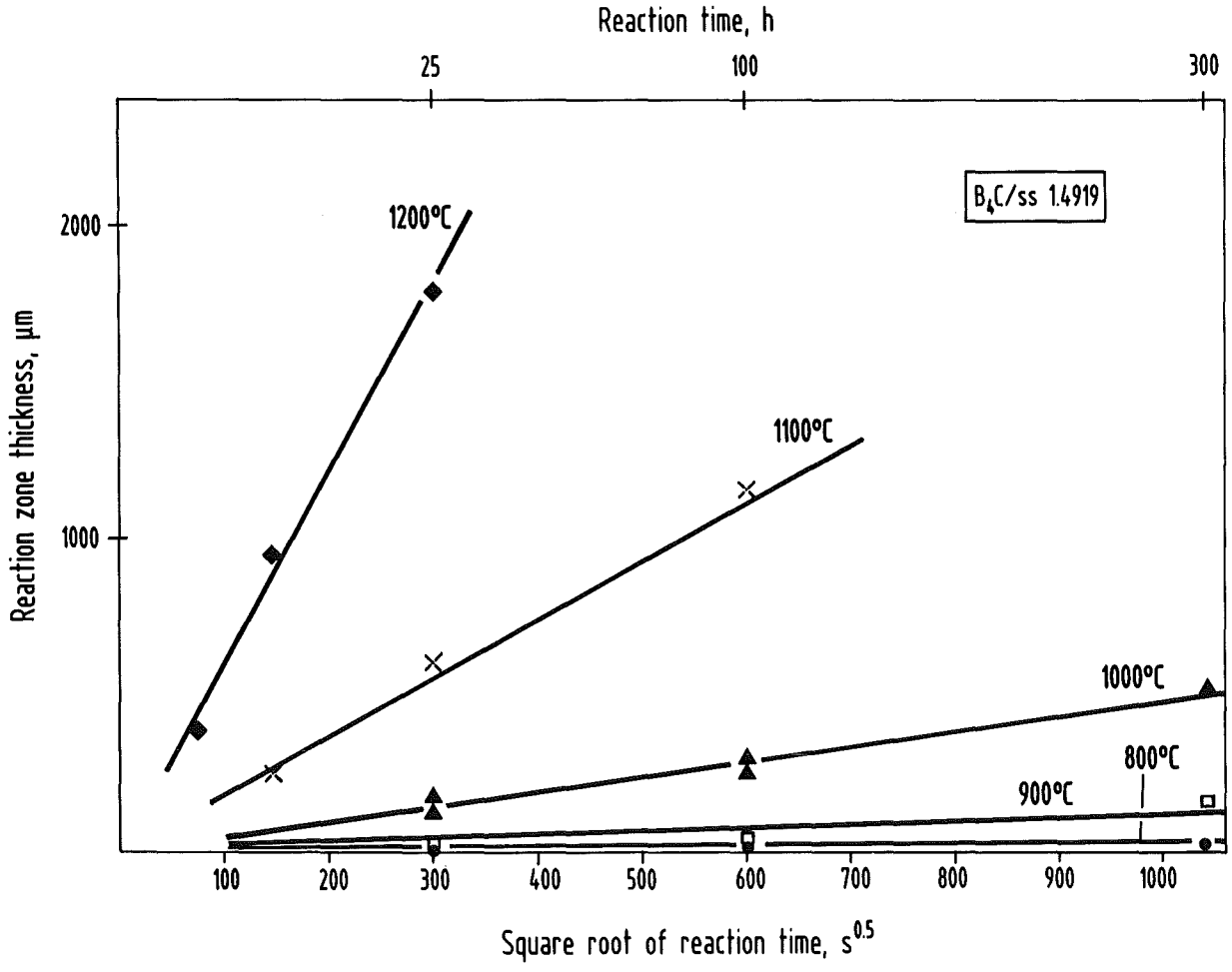

Fig. 5: Overall reaction zone thicknesses in the B_4C/stainless steel reaction couple for 800 - 1200 °C.

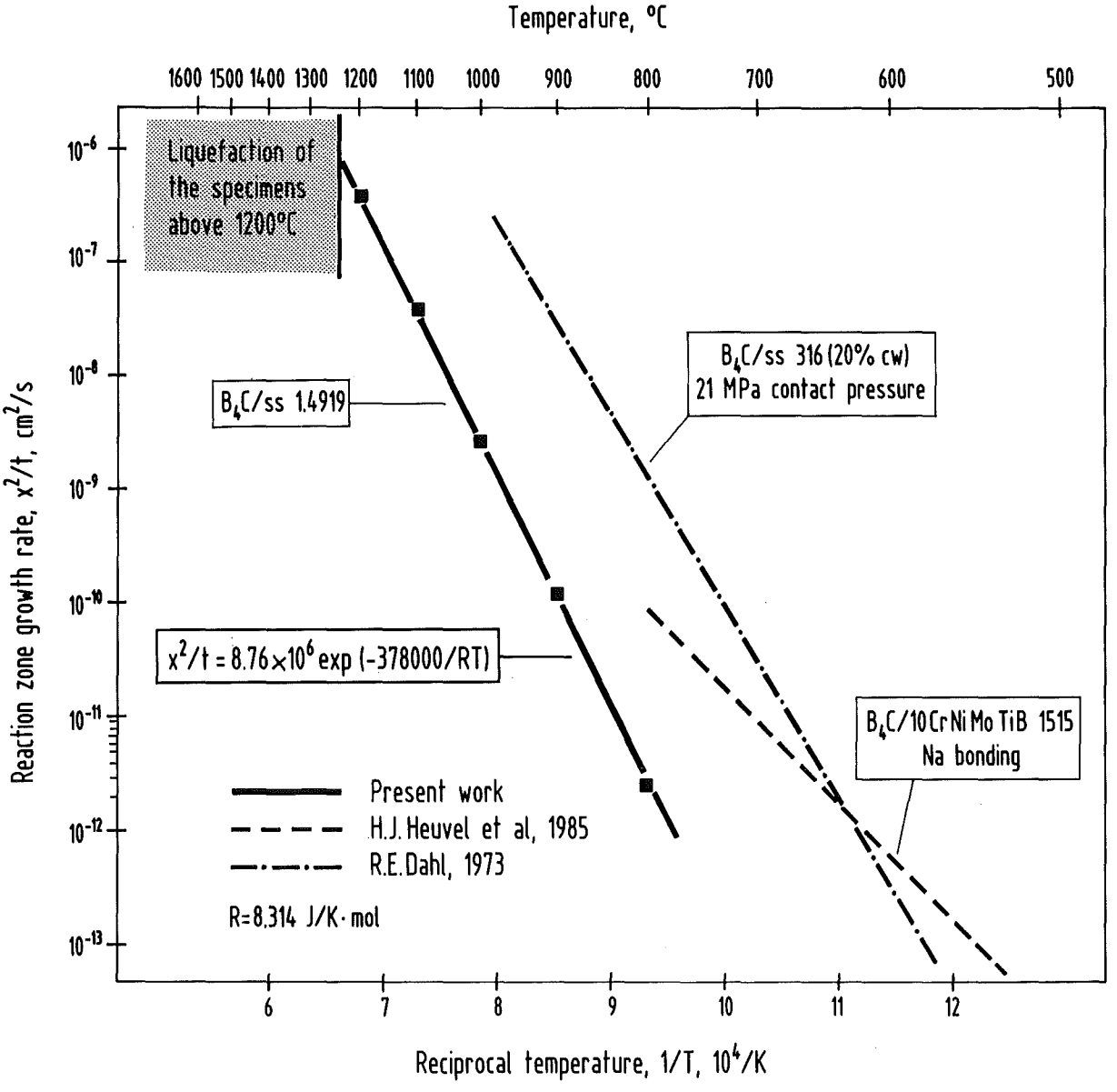

Fig. 6: Reaction zone growth rates in the B_4C/stainless steel reaction couple for 800 - 1200 °C. Comparison with literature data [5,6].

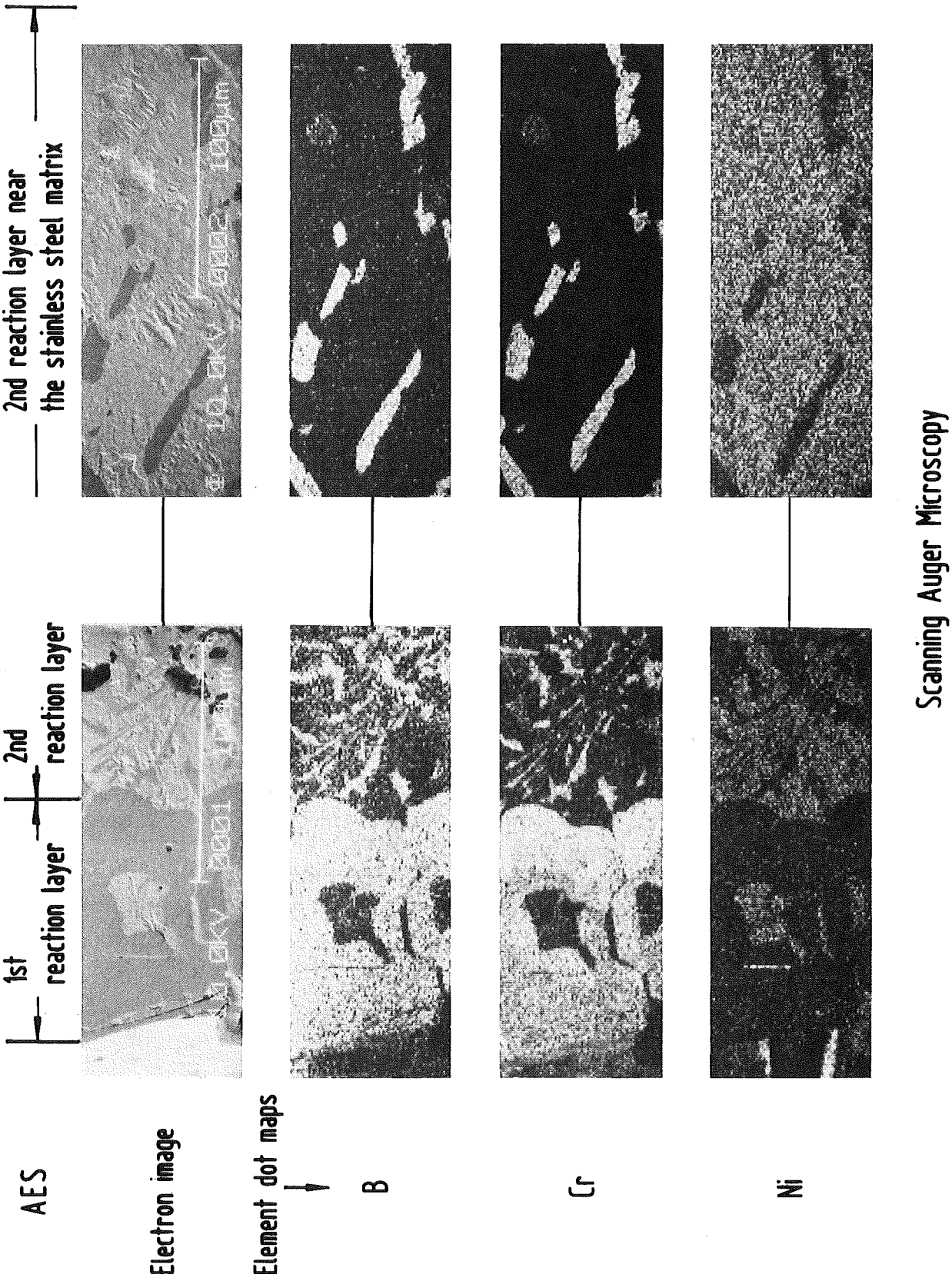

Fig. 7: Chemical composition of the B_4C/stainless steel reaction zones after 6 h at 1200 °C. The Fe and C element dot maps are not shown.

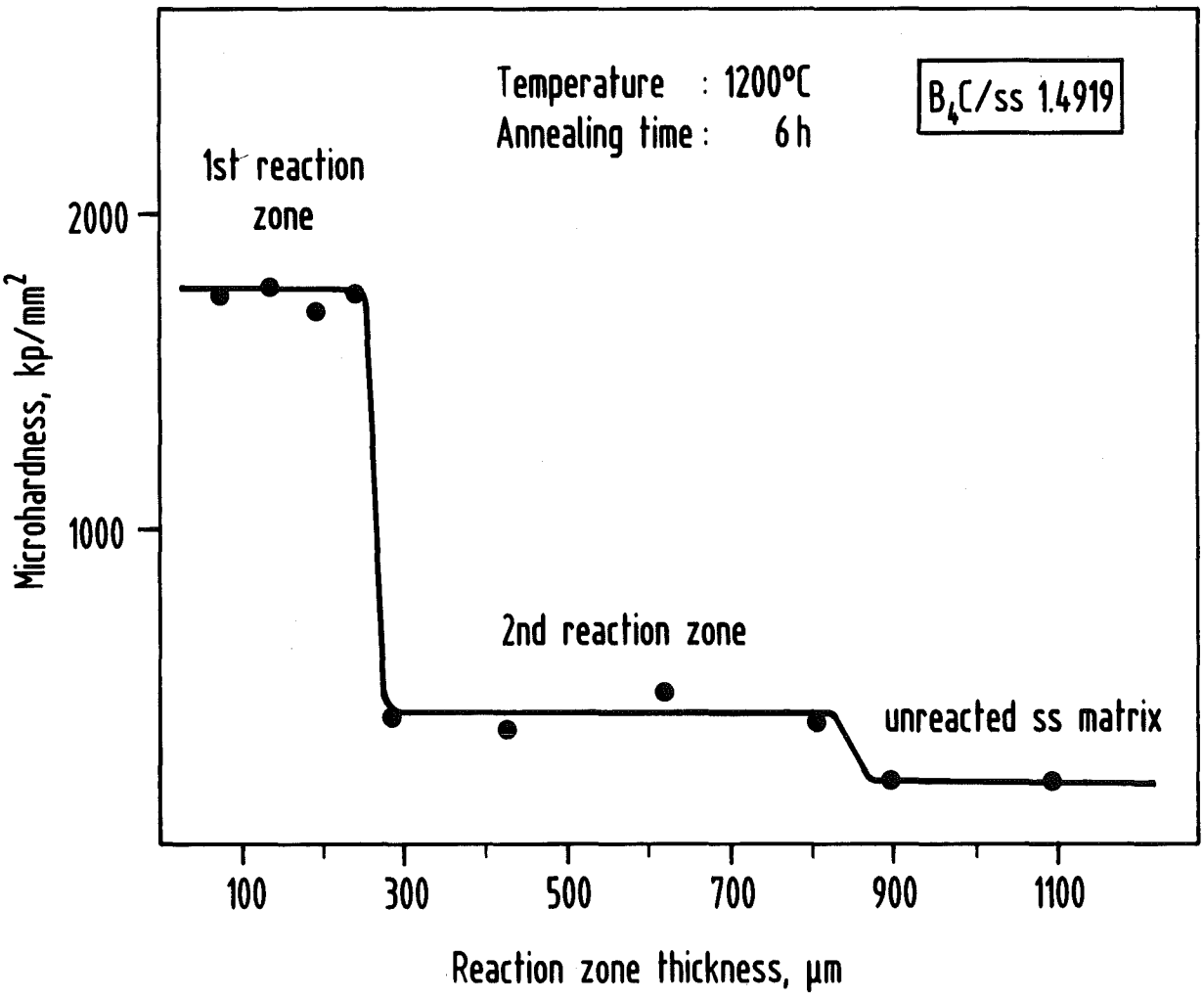

Fig. 8: Microhardness of B_4C/stainless steel reaction zones.

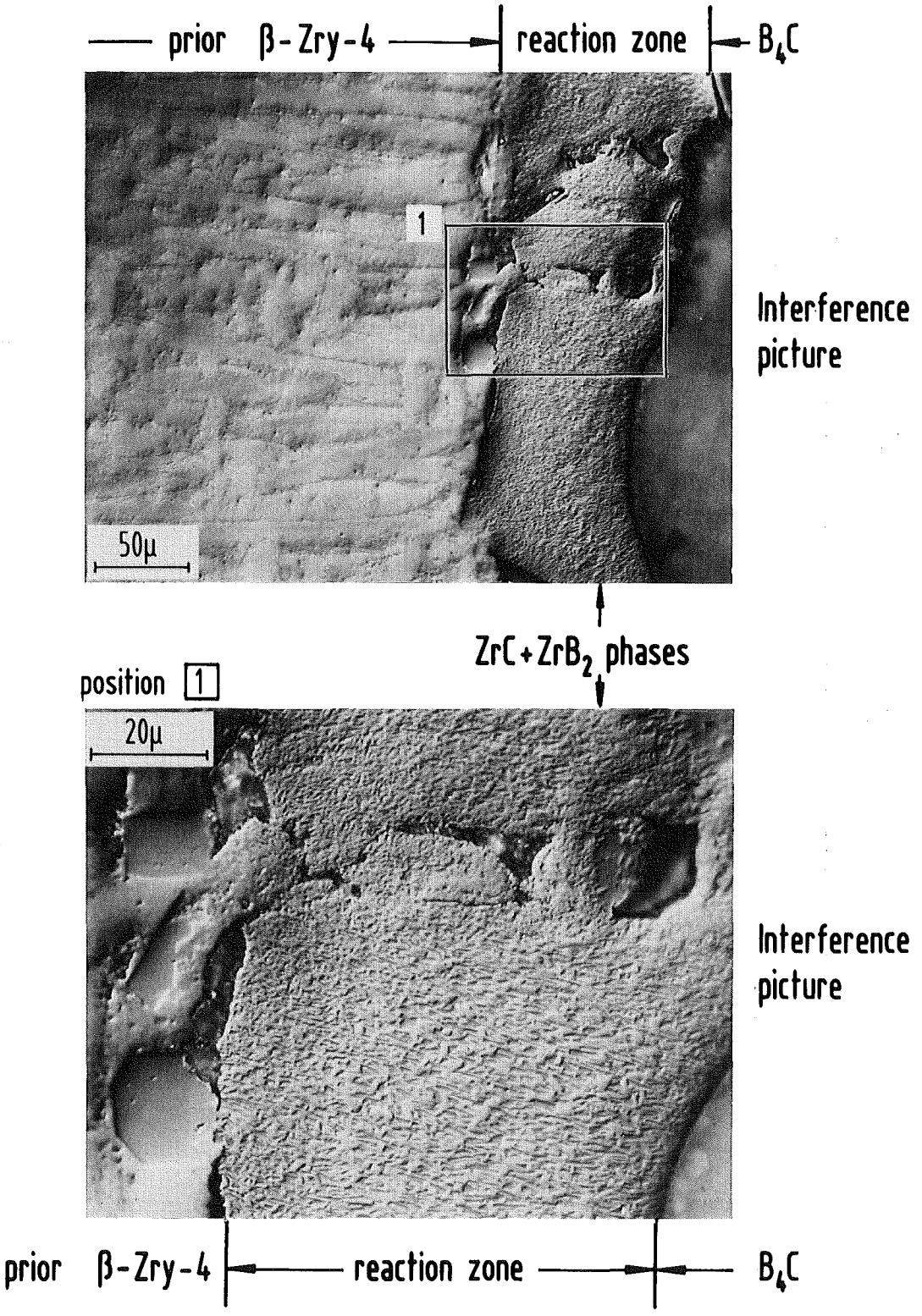

Fig. 9: Appearance of the B_4C/Zircaloy-4 reaction zone after 300 h at 1100 °C.

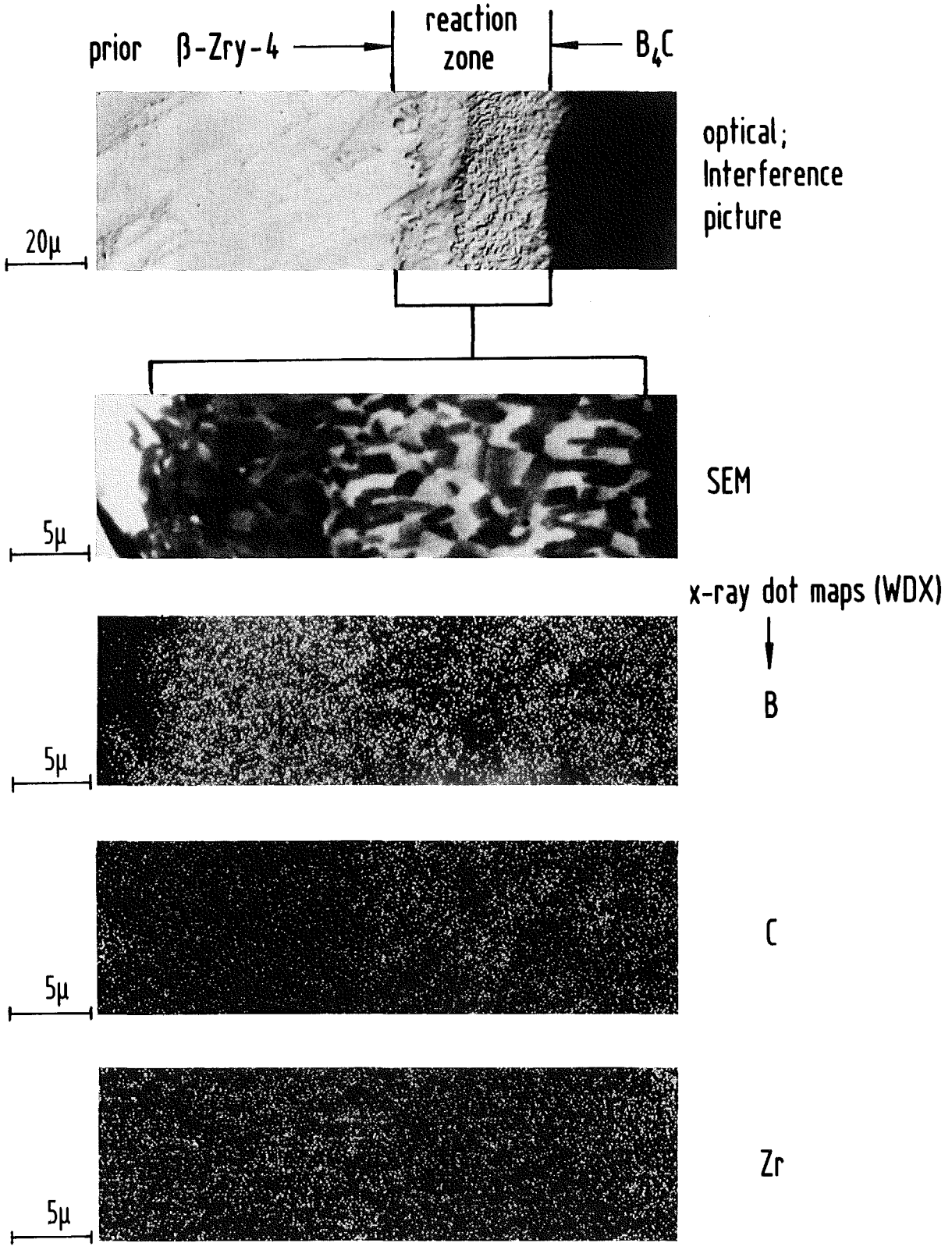

Fig. 10: Chemical composition of the B_4C/Zircaloy-4 reaction zones after 1 h at 1500 °C.

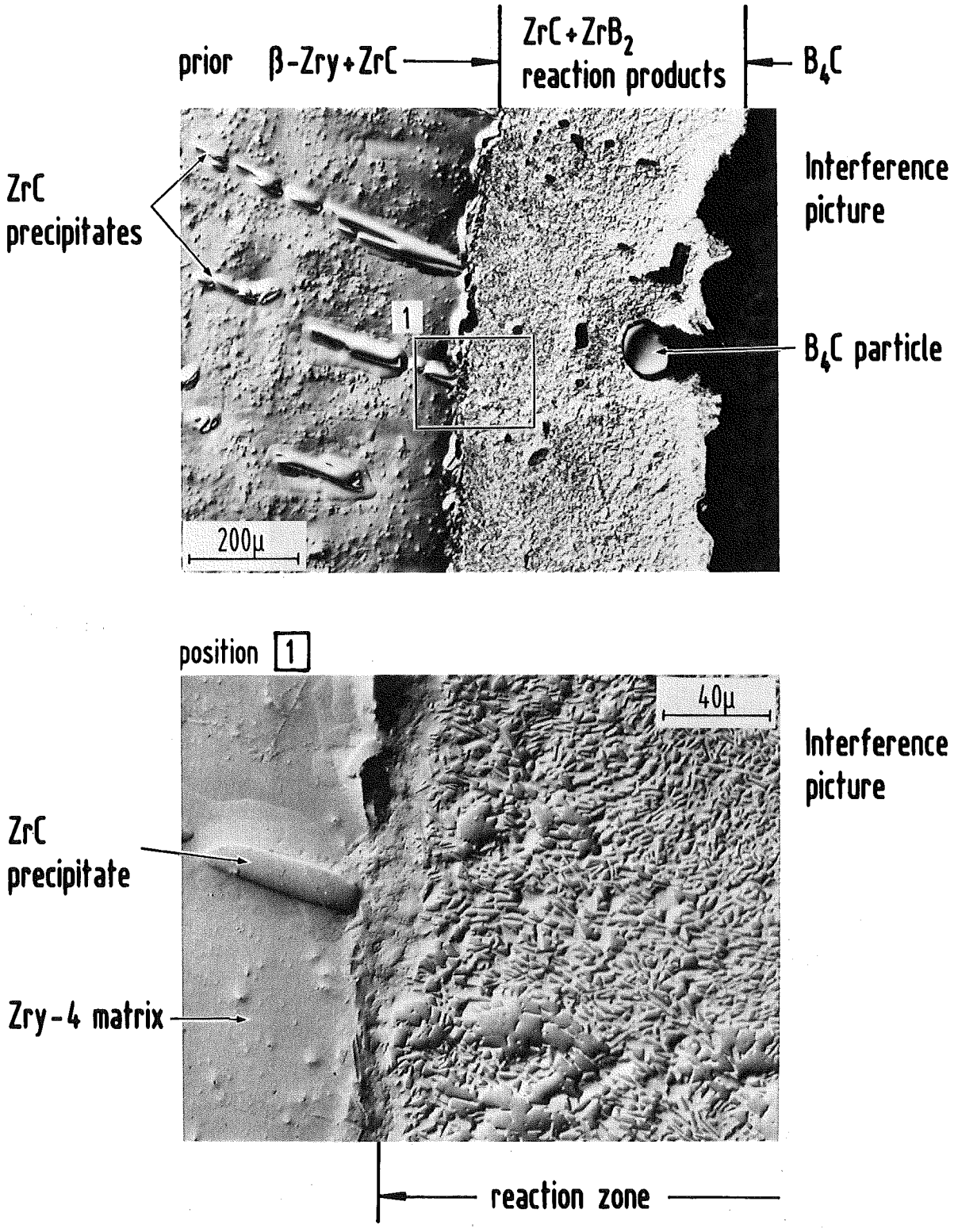

Fig. 11: Appearance of the B_4C/Zircaloy-4 reaction zone after 6 h at 1600 °C.

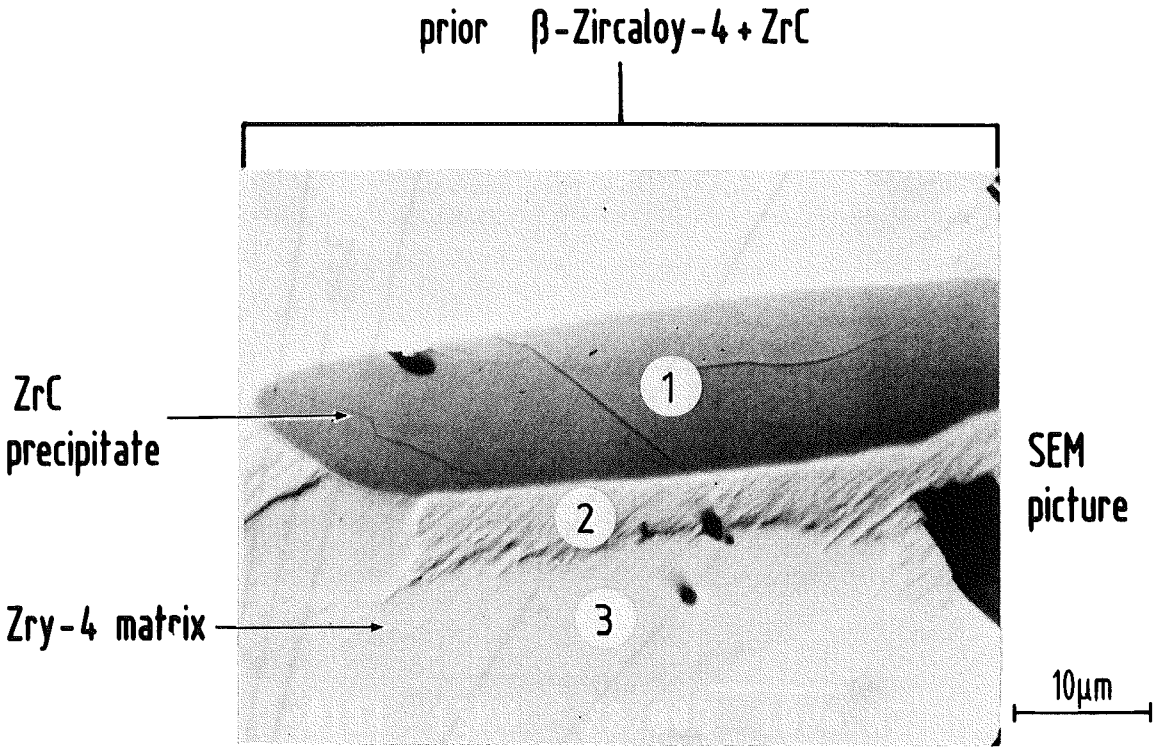

SEM/WDX Analysis (counts/sec)

Element	1	2	3
B	10	~	~
C	135	42	30
O	72	71	62

Fig. 12: ZrC precipitate within the Zircaloy-4 matrix of a B_4C/Zircaloy-4 reaction couple after 6 h at 1600 °C.

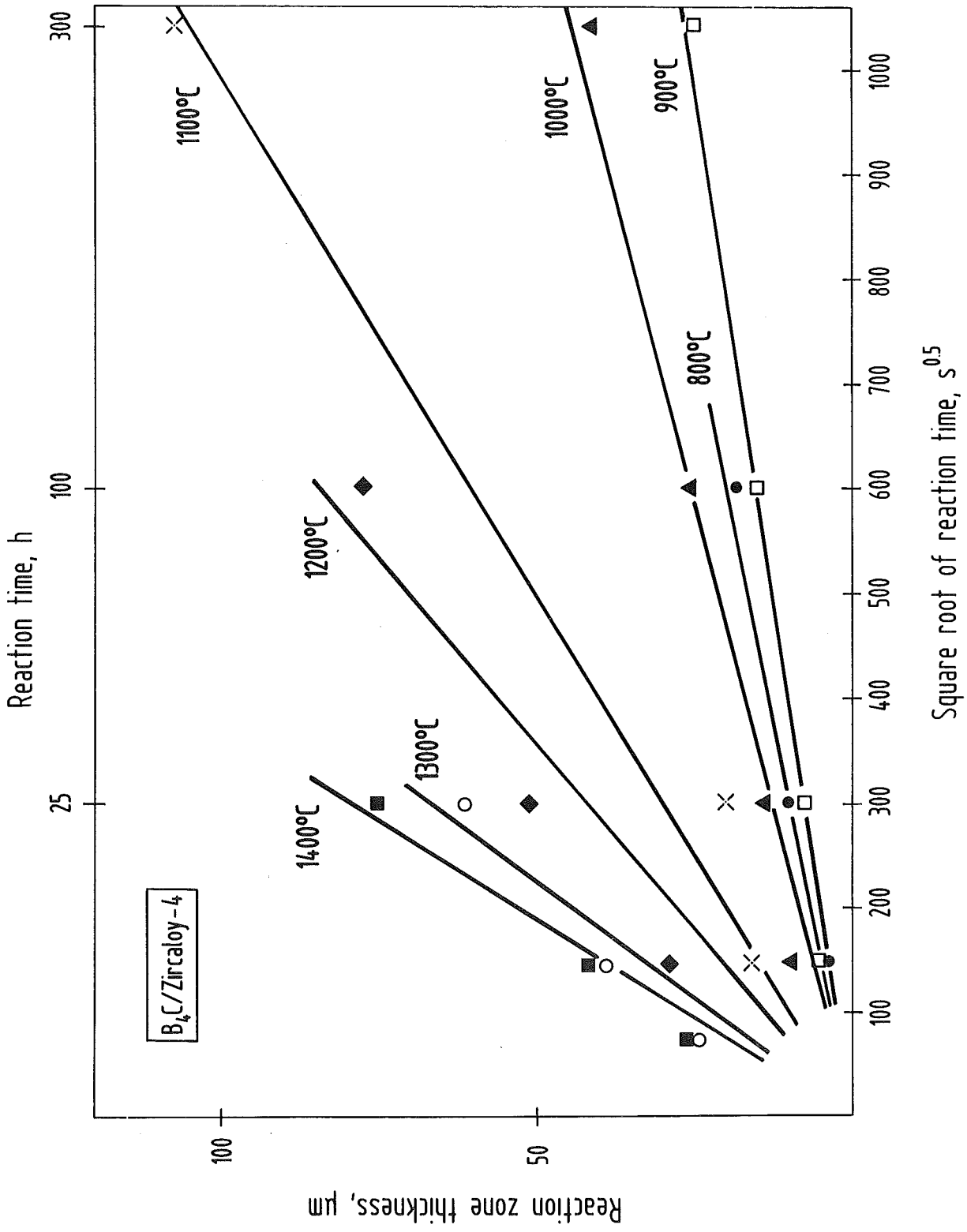

Fig. 13: Overall reaction zone thicknesses in the B_4C/Zircaloy-4 reaction couple for 800 - 1200 °C.

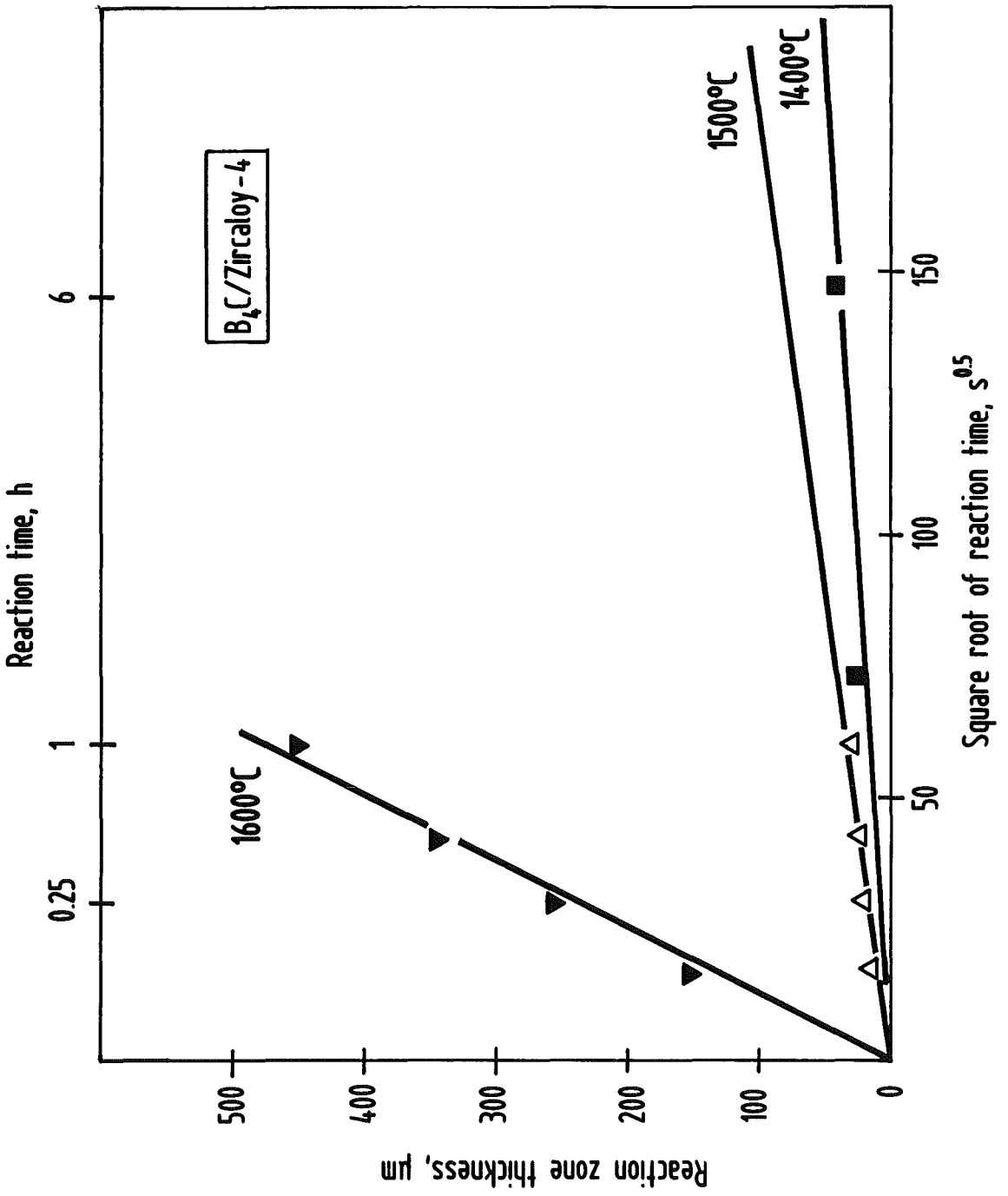

Fig. 14: Overall reaction zone thicknesses in the B_4C/Zircaloy-4 reaction couple for 1400 - 1600 °C.

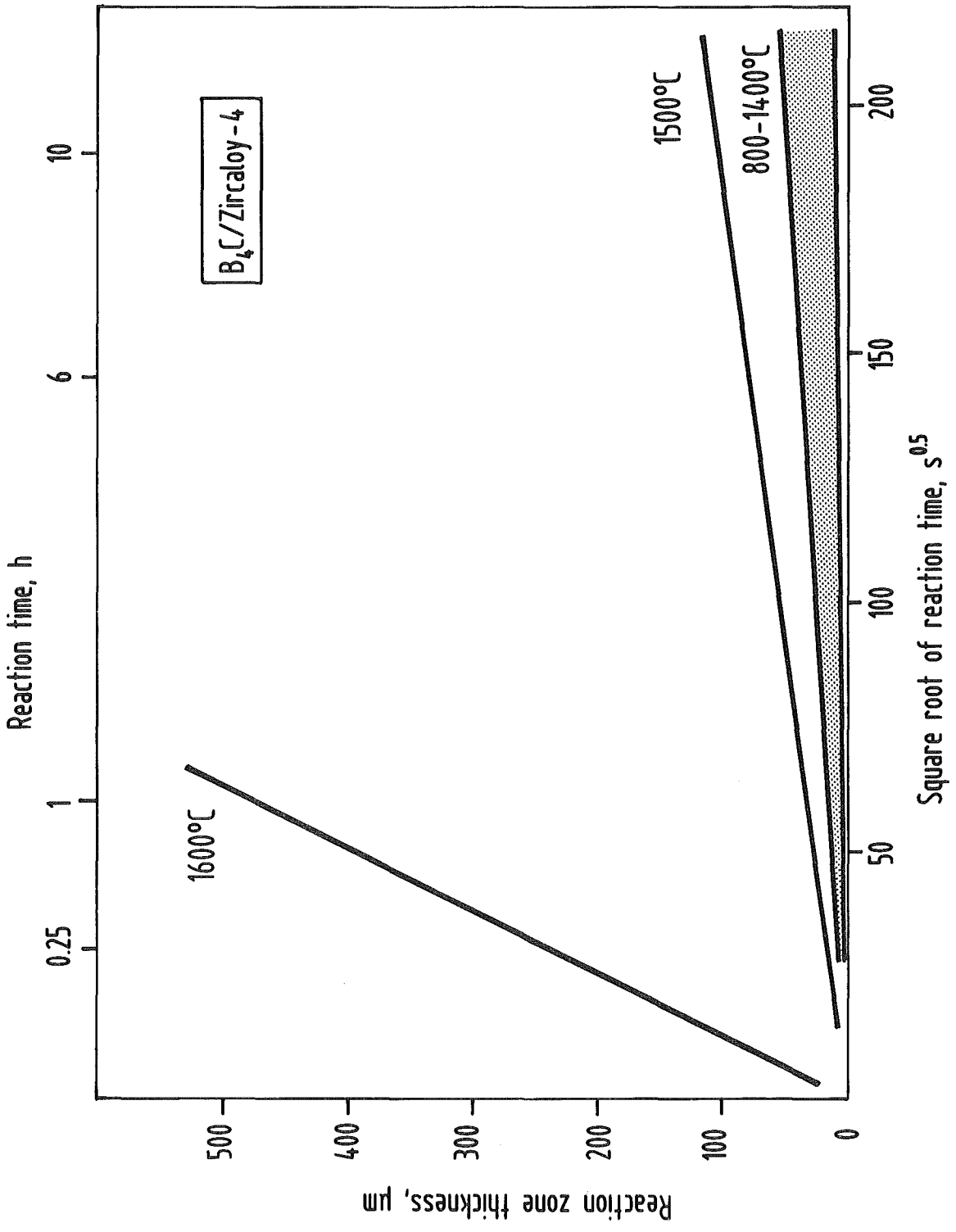

Fig. 15: Overall reaction zone thicknesses in the B_4C/Zircaloy-4 reaction couple for 800 - 1600 °C.

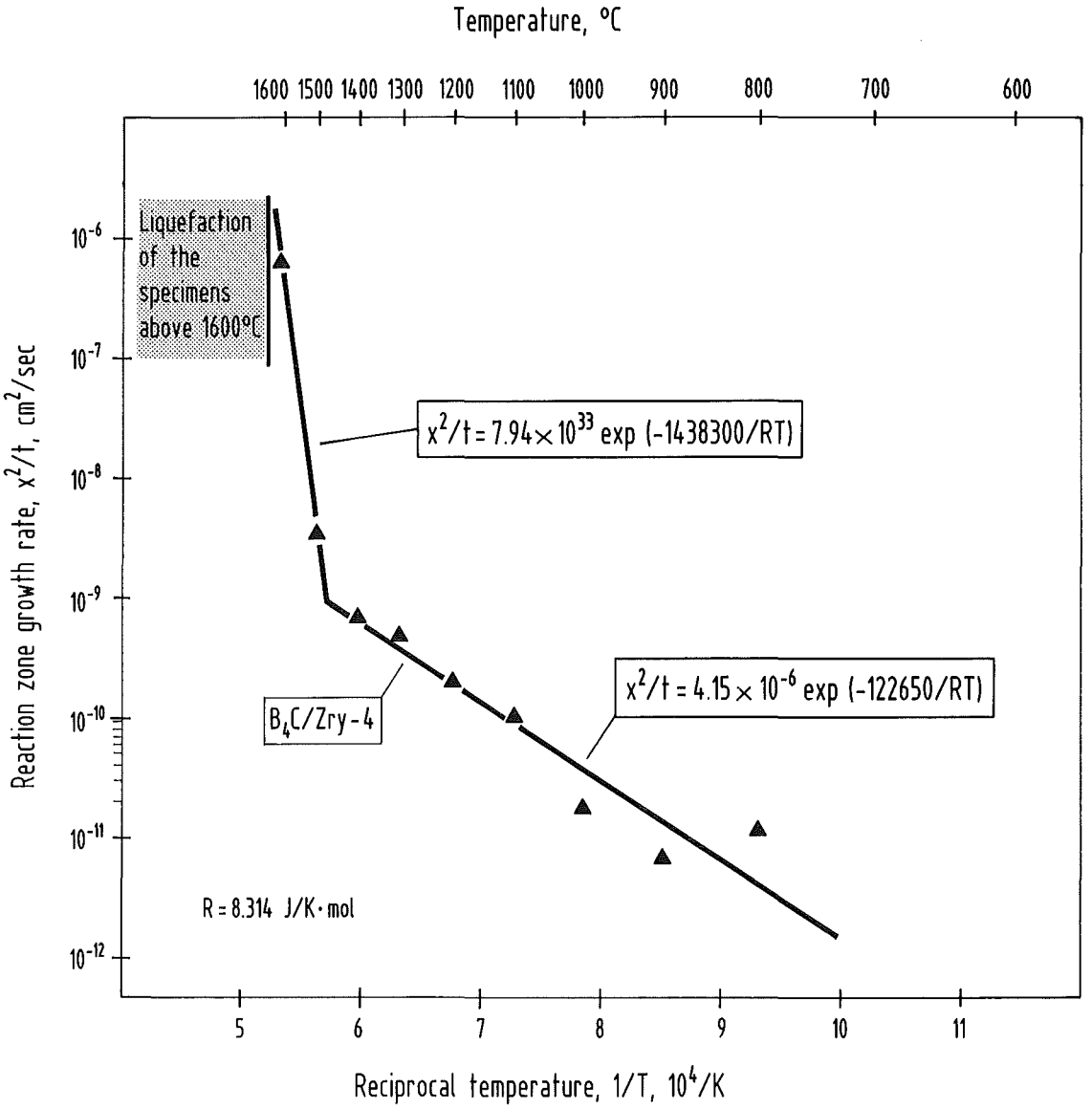

Fig. 16: Reaction zone growth rates in the B_4C/Zircaloy-4 reaction couple for 800 - 1600 °C.

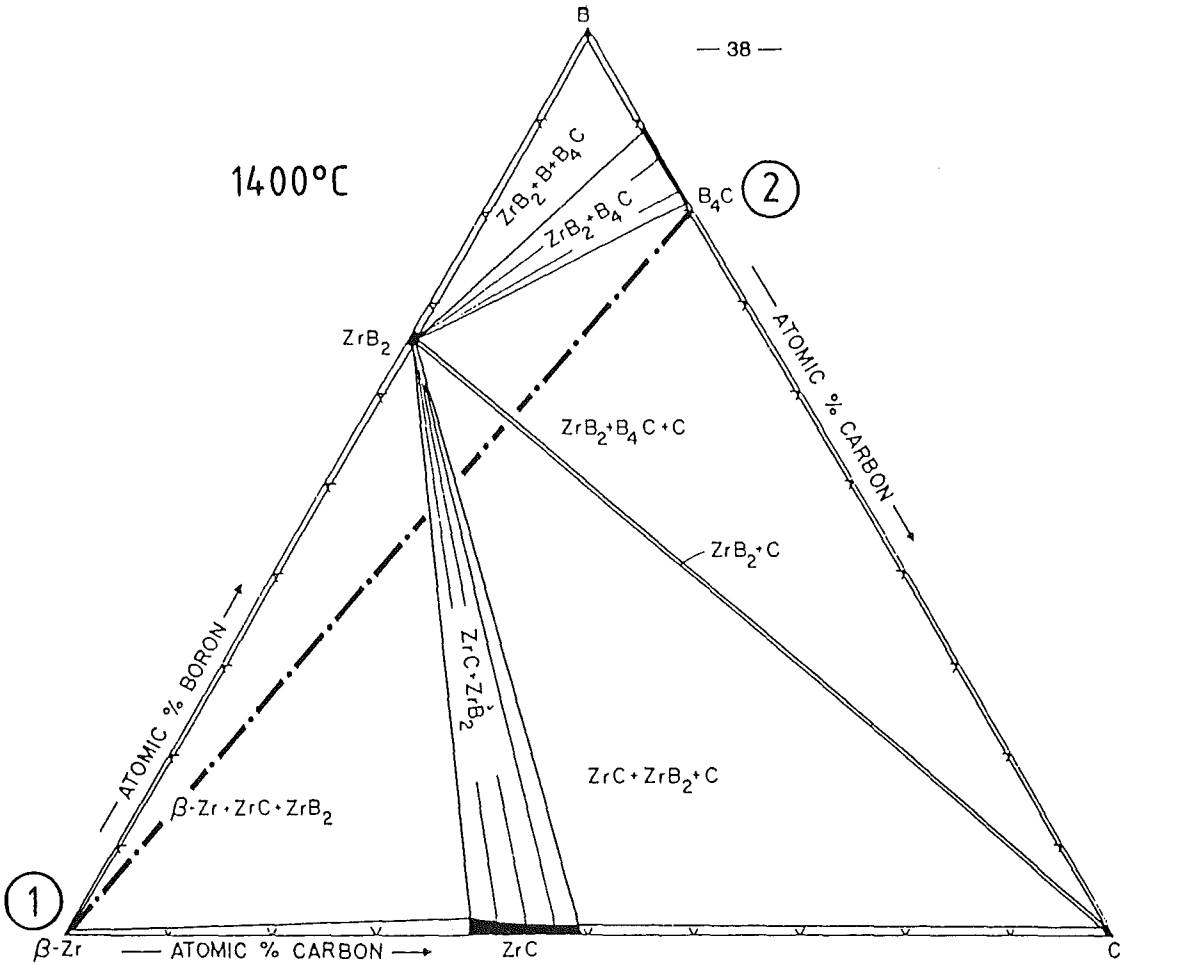

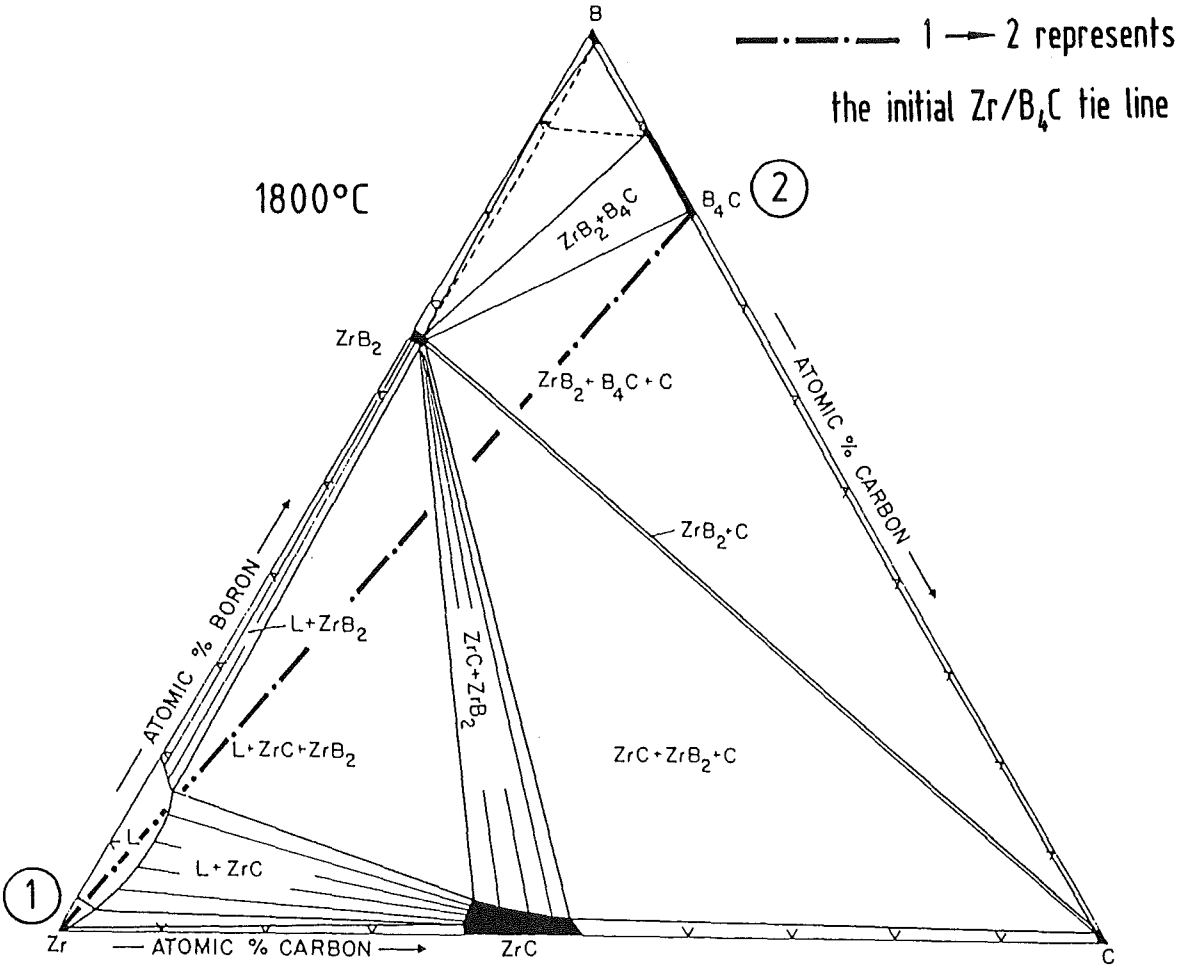

Fig. 17: Isothermal section of the Zr-B-C system at 1400 °C (upper picture) and 1800 °C (lower picture) [8].

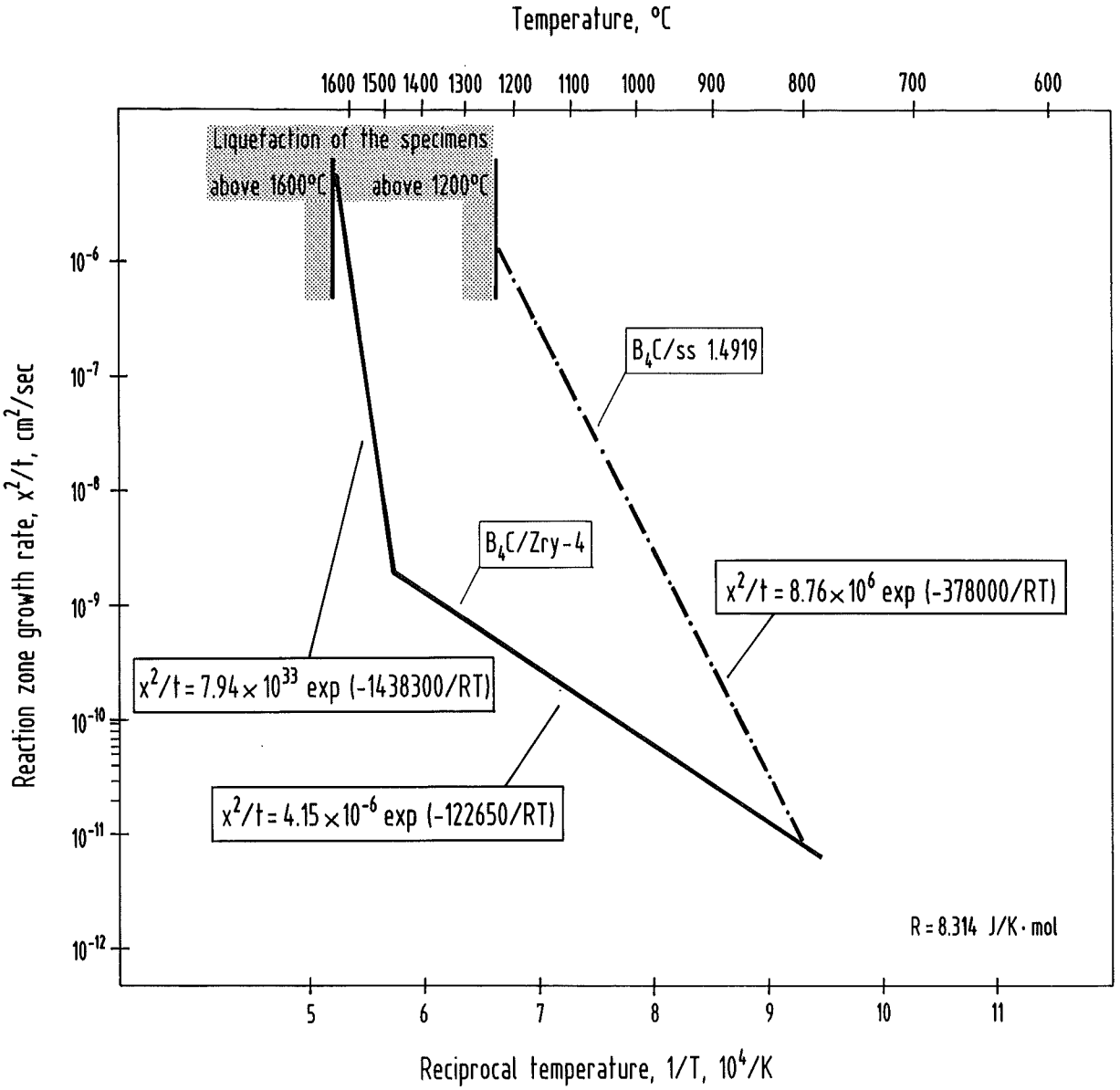

Fig. 18: Comparison of the reaction zone growth rates of the reaction couples B_4C/stainless and B_4C/Zircaloy-4.

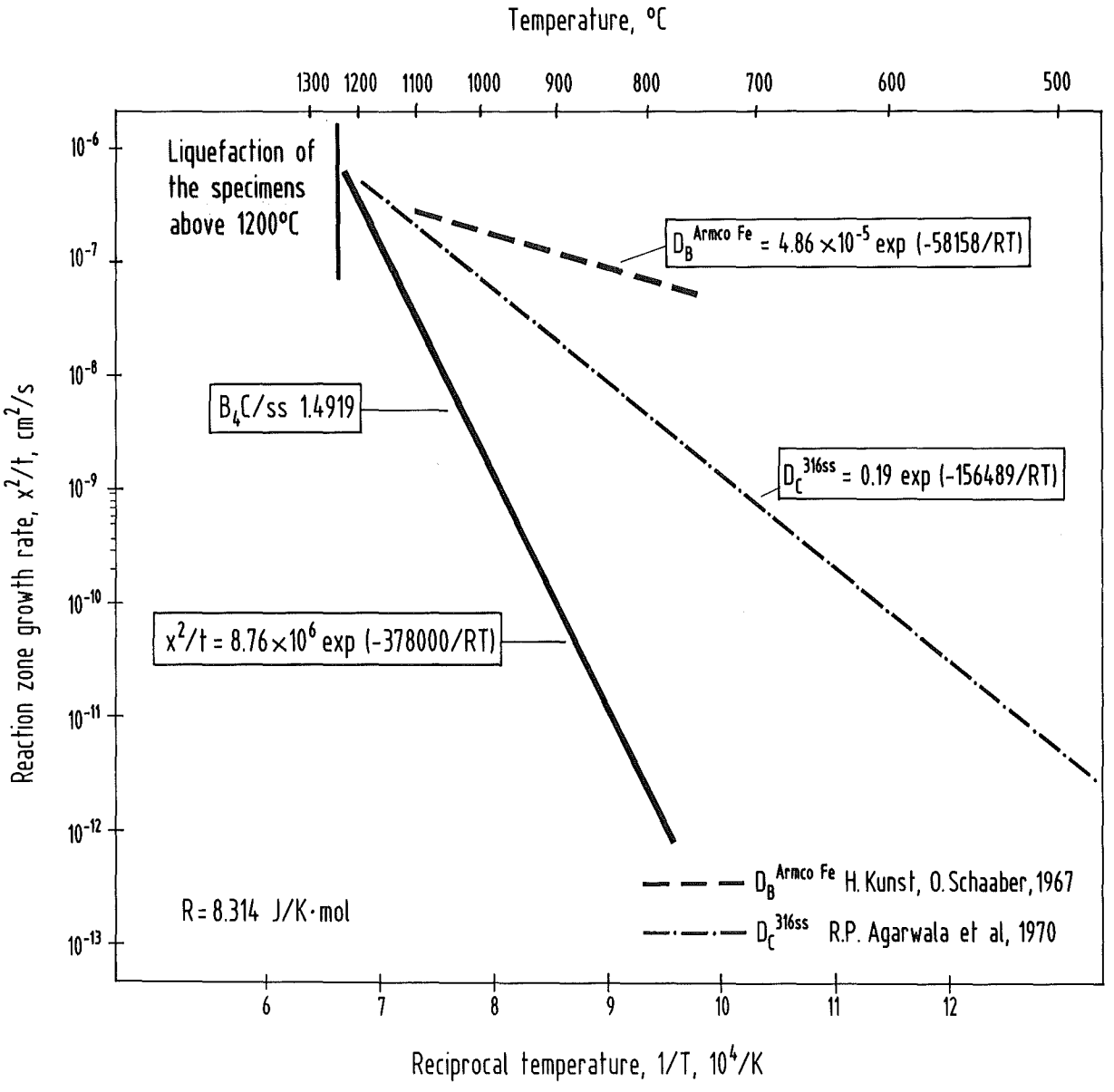

Fig. 19: Comparison of the reaction zone growth rates in the B_4C/stainless steel reaction couple with those of the boron diffusion in Armco Fe and the carbon diffusion in stainless steel 316 [9,10].

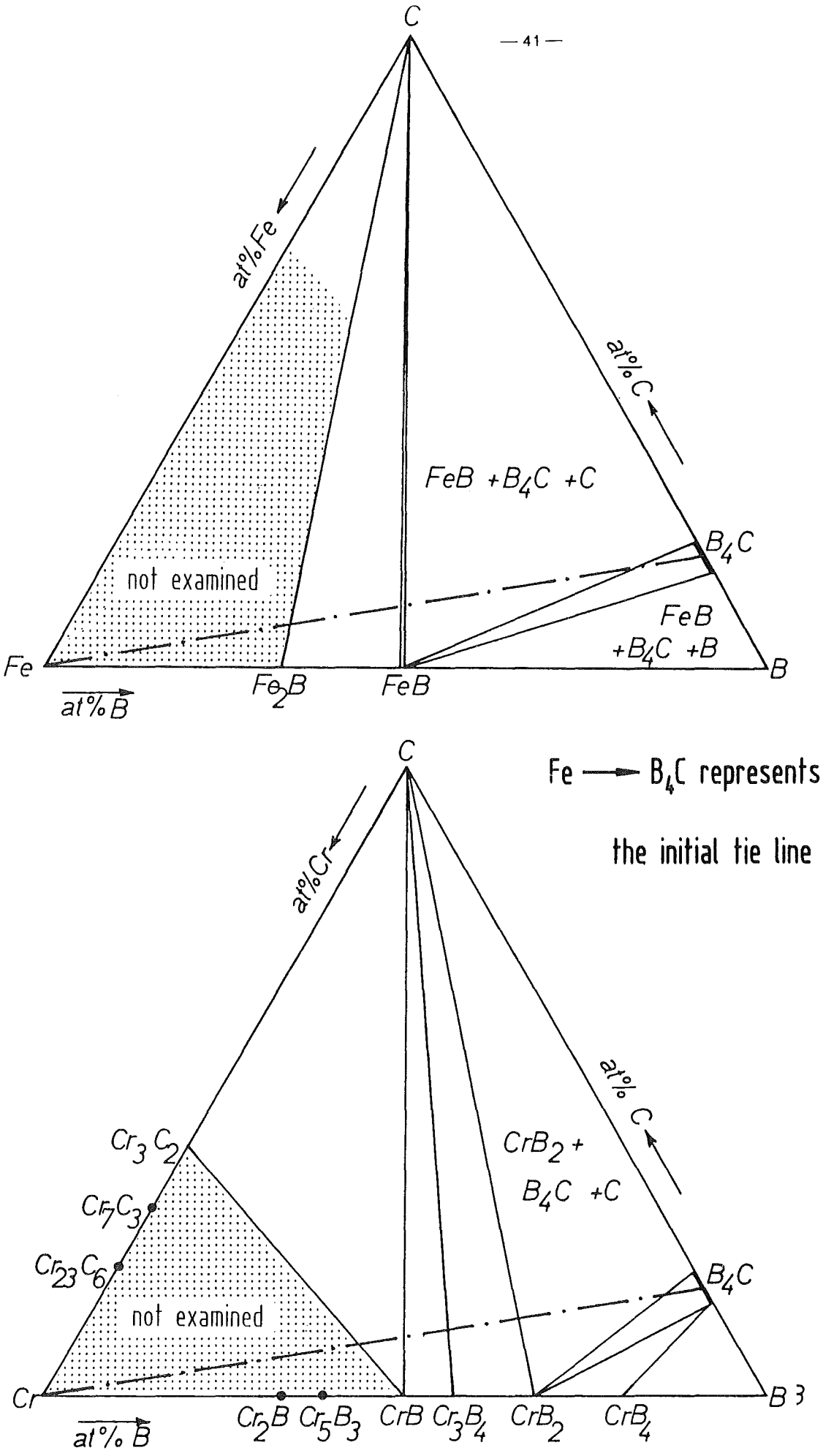

Fig. 20: Isothermal section of the Fe-C-B system at 1000 °C (upper picture) and the Cr-C-B system at 1100 °C (lower picture) [15].

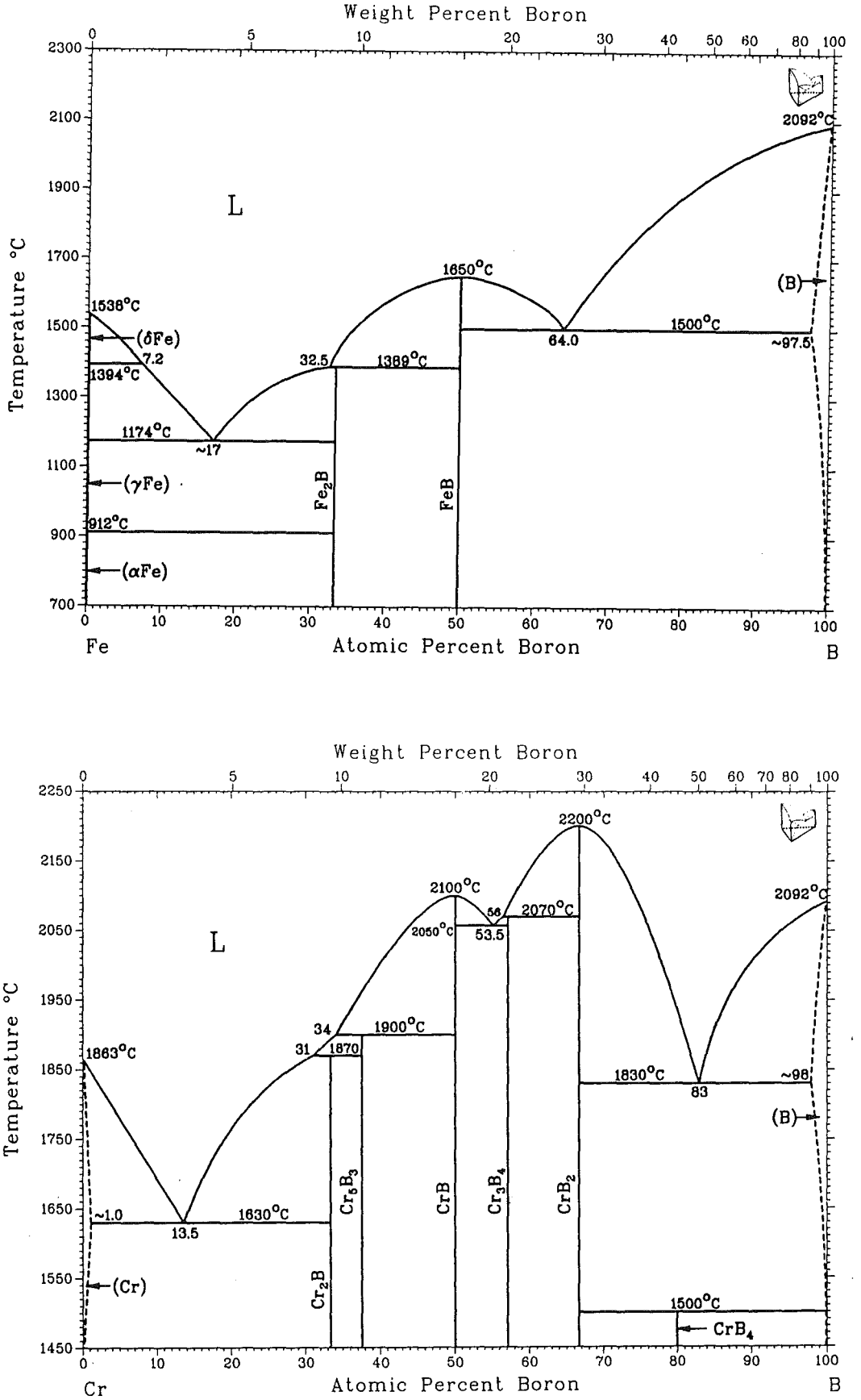

Fig. 21a: Binary alloy phase diagrams of the systems Fe-B, Cr-B, and Ni-B [13].

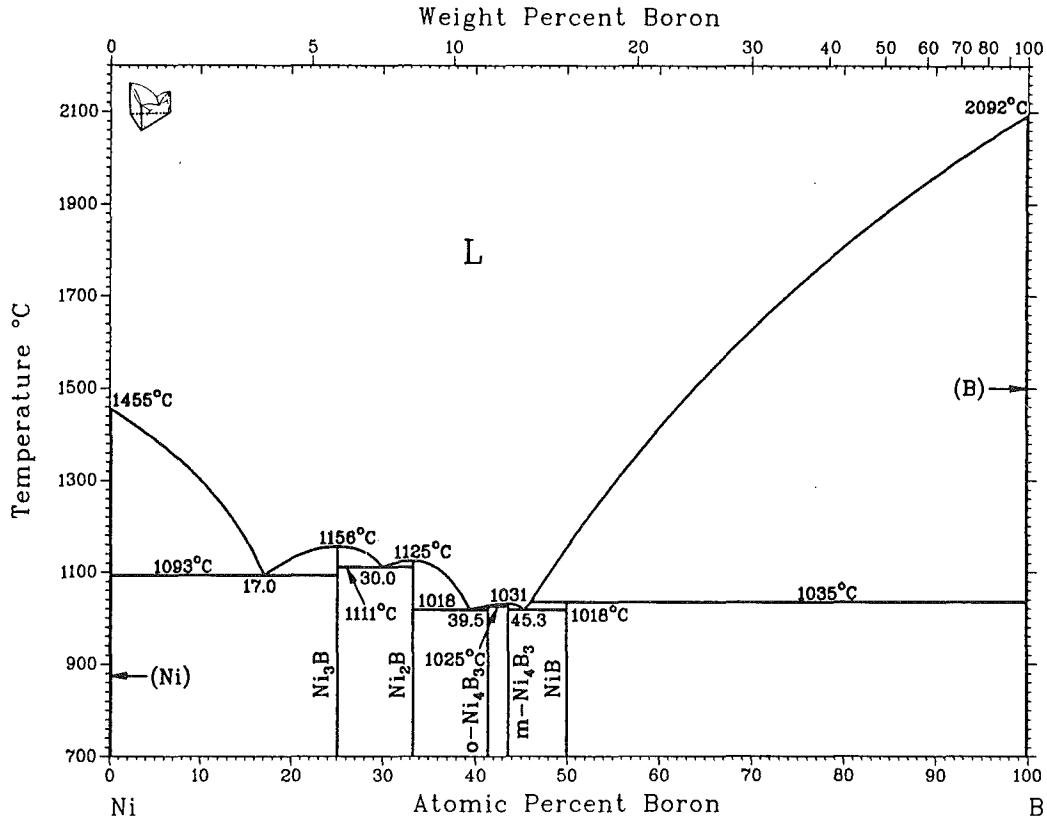

Fig. 21b: Binary alloy phase diagrams of the systems Fe-B, Cr-B, and Ni-B [13].

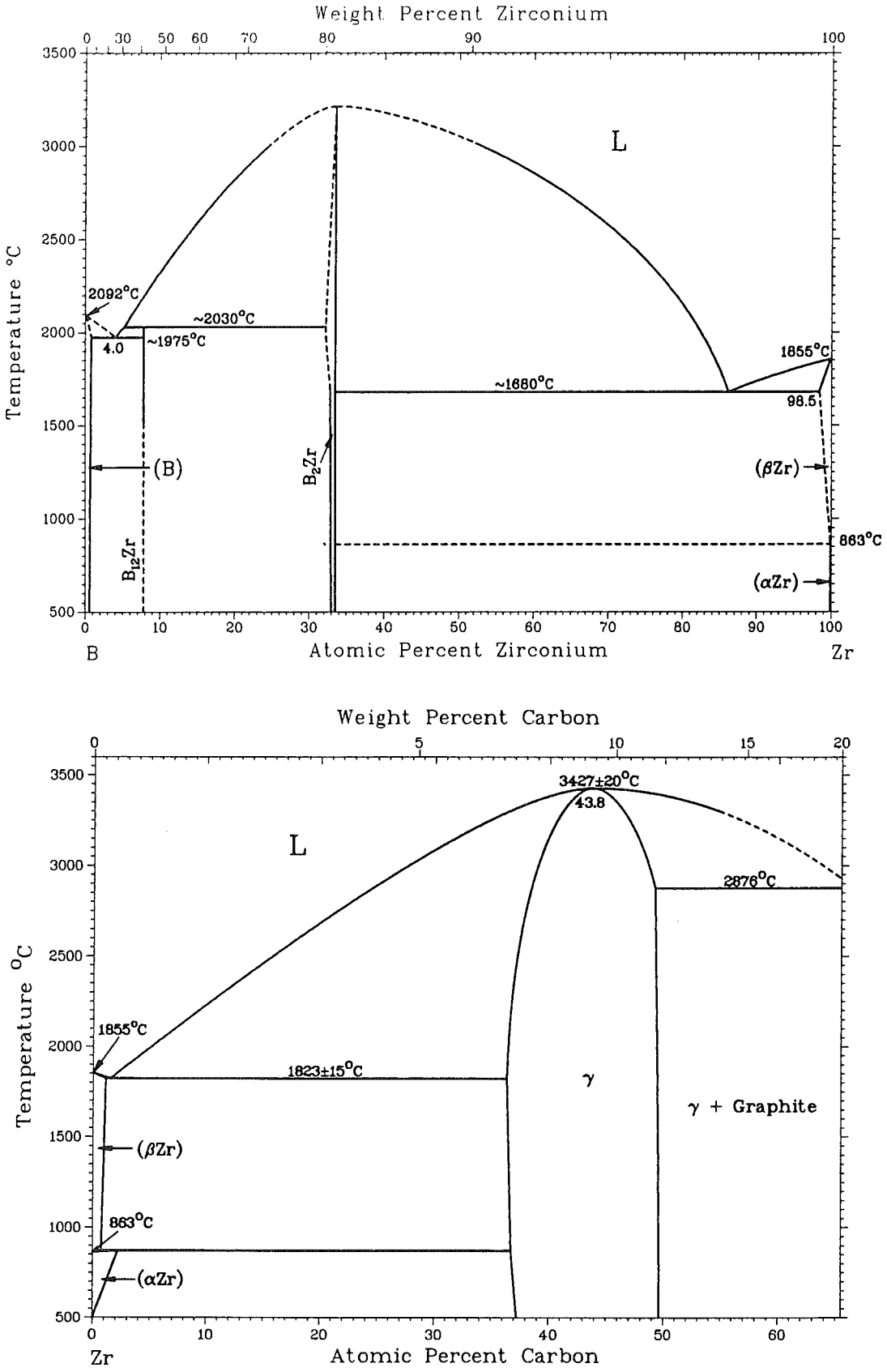

Fig. 22: Binary alloy phase diagrams of the systems Zr-B and Zr-C [13].

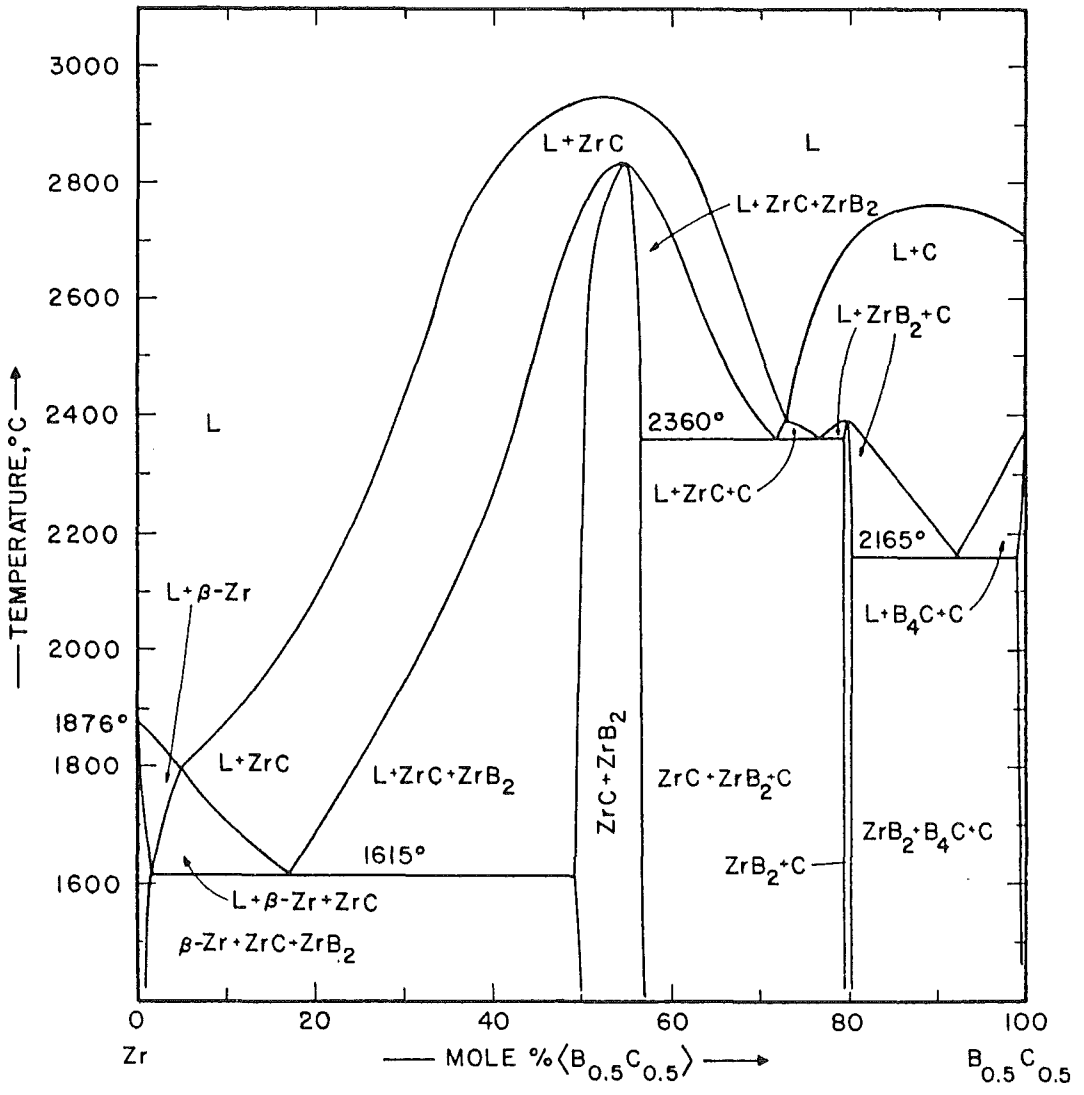

Fig. 23: Phase relations in the pseudo binary phase system Zr-($B_{0.5}C_{0.5}$) [8].